AD NUMBER
ADC016220
CLASSIFICATION CHANGES
TO: unclassified
FROM: secret
LIMITATION CHANGES
TO: Approved for public release, distribution unlimited
FROM: Distribution limited to U.S. Gov't. agencies only; Test and Evaluation; Sep 78. Other requests for this document must be referred to Commanding Officer, Naval Research Lab., Washington, DC 20375.
AUTHORITY
NRL ltr, 3 Mar 2004; NRL ltr, 3 Mar 2004

(2) LEVEL II

SECRET

NRL Memorandum Report 3832
Copy 076 of 100 Copies

Preliminary Results of an Analysis of Beam Noise in the Mediterranean

[Unclassified Title]

R. Heitmeyer and G. Long

Large Aperture Acoustics Branch
Acoustics Division

"NATIONAL SECURITY INFORMATION"

"Unauthorized Disclosure Subject to Criminal Sanctions"

September 1978

NAVAL RESEARCH LABORATORY
Washington, D.C.

SECRET: Classified by CNO OP955F1
Exempt from GDS of E.O. 11652
Ex. Cat. (3) Auto Declass. Dec. 31, 2006

SECRET

NATIONAL SECURITY INFORMATION

Unauthorized Disclosure Subject to Criminal Sanctions.

NAVAL RESEARCH LABORATORY
WASHINGTON, D.C. 20375

IN REPLY REFER TO:
8160-280:RMH:ng
SER:

REGISTERED
SECRET--Unclassified upon removal of enclosure (1)

From: Commanding Officer, Naval Research Laboratory, Washington, D.C. 20375
To: Distribution List

Subj: NRL Memorandum Report - Beam Noise Analysis (U)

Encl: (1) (S) Preliminary Results of an Analysis of Beam Noise in the Mediterranean (U)

1. (U) The Long Range Acoustic Propagation Project (LRAPP) of the Naval Ocean Research Development Activity (NORDA) sponsored a study, to analyze data, during the period January 1977 to September 1977.

2. (U) Enclosure (1) is a report of the results of that study. As authorized by the Director, LRAPP, enclosure (1) is forwarded for your information and retention.

John C Munson

Distribution:
Assistant Secretary of the Navy (RE and S)
CNO (OP-095, OP-951, OP-955)
NAVELEX (PME-124/30, 124/40, 124/60, ELEX 320, ELEX 035)
NOSC (Codes 714, 531)
CNA (C.E. Woods)
NAVMAT (MAT-035)
NSRDC
NAVAIRDEVCEN
CINLANTFLT
COMOCEANSYSLANT

8160-280:RMH:ng
SER:

UNCLASSIFIED

Distribution:
ONR (J. Hersey)
OCEANAV
NAVAIRSYSCOM (PMA-264)
NAVSEA SYSCOM (SEA-06H1)
DIRSSPO WASH DC
PROJMGR ASWS
NAVOCEANO
DDC
DARPA
ARC (E.L. Smith)
NORDA (Codes 110, 200, 300, 320, 340, 400, 500, 600)
NORDA LO (Code 100N)
NUSC (R.L. Martin)
MASWSPO (PM-4)
A&T (S. Elam)
APL/JHU (Dr. G. L. Smith)
ADL (Dr. G.R. Raisbeck)
DSC
PSI
SAI (Dr. J.S. Hanna)
SUTRON (C.H. Dabney)
TETRA/TECH (W.E. Sims, J.R. Preston)
TI (A. Kirst, Jr.)
TRACOR (J.T. Gottwald, Dr. A.F. Wittenborn)
TRW (I.B. Gereben)
URC
USI (Dr. M.S. Weinstein)
ARL/UT (G.E. Ellis, Dr. L.D. Hampton)
XONICS INC (S. Kulek)
WHOI (E. Hays)
WECO
RATHEON (B. Becker)
ORI (J. Brown)
MPL/UC (V. Anderson)
OHW
BTL
BBN
NRL (Code 8160)

SECRET

SECURITY CLASSIFICATION OF THIS PAGE (When Date Entered)

REPORT DOCUMENTATION PAGE

READ INSTRUCTIONS BEFORE COMPLETING FORM

1. REPORT NUMBER: NRL Memorandum Report 3832	2. GOVT ACCESSION NO
3. RECIPIENT'S CATALOG NUMBER	
4. TITLE (and Subtitle): Preliminary Results of an Analysis of Beam Noise in the Mediterranean (U). [Unclassified Title]	5. TYPE OF REPORT & PERIOD COVERED: Interim report on a continuing NRL problem
	6. PERFORMING ORG. REPORT NUMBER
7. AUTHOR(s): Richard Heitmeyer and Gordon Long	8. CONTRACT OR GRANT NUMBER(s): NORDA 63795N, R0S17
9. PERFORMING ORGANIZATION NAME AND ADDRESS: Naval Research Laboratory, Washington, D.C. 20375	10. PROGRAM ELEMENT, PROJECT, TASK AREA & WORK UNIT NUMBERS: 81S01-38
11. CONTROLLING OFFICE NAME AND ADDRESS: Naval Ocean Research and Development Activity, Long Range Acoustic Propagation Project, NSTL Station, Miss. 39520	12. REPORT DATE: September 1978
	13. NUMBER OF PAGES: 58
14. MONITORING AGENCY NAME & ADDRESS (If different from Controlling Office): NRL-MR-3832	15. SECURITY CLASS. (of this report): SECRET
	15a. DECLASSIFICATION DOWNGRADING SCHEDULE: XGDS-3-2006

16. DISTRIBUTION STATEMENT (of this Report)
Distribution limited to Government Agencies; Test and Evaluation; September 1978. Other requests for this document must be referred to the Commanding Officer, Naval Research Laboratory, Washington, D.C. 20375.

17. DISTRIBUTION STATEMENT (of the abstract entered in Block 20, if different from Report)

18. SUPPLEMENTARY NOTES

19. KEY WORDS (Continue on reverse side if necessary and identify by block number)
Ambient Noise Directionality
Spatial Statistics
Towed Array System
LAMBDA II Array
Mediterranean Noise

20. ABSTRACT (Continue on reverse side if necessary and identify by block number)
(S) The beam noise measured on the LAMBDA II array system in the Mediterranean Sea is currently being analyzed in two 30 Hz frequency bands: A 275-305 Hz band and a 30-60 Hz band. The preliminary results of that analysis, ~~reported herein,~~ indicate that the beam noise in the HF band, as well as the MF band, is primarily due to shipping. The variation with azimuth in both frequency bands is in qualitative agreement with ship location data. There are, however, many instances where different noise sources contribute in each band,

DD FORM 1 JAN 73 1473 EDITION OF 1 NOV 65 IS OBSOLETE

SECRET

SECURITY CLASSIFICATION OF THIS PAGE (When Data Entered)

251 150

(S)indicating the presence of more than one (Acoustic) ship class. The beam noise in the HF band exhibits fewer spectral lines than in the MF band and the power in those lines is distributed over a smaller range. As a consequence, the extent of the line clutter due to false targets is a more sensitive function of the detection threshold. This result, together with the results of an earlier analysis, suggests that the 300 Hz line of a Type II target can be detected in a low clutter environment, but that the 50 Hz line should rarely be visible and then only in a high clutter environment. Finally, an algorithm is described which significantly reduces the error in the beam noise that results from three missing hydrophones in the otherwise, equally spaced, HF array segment.

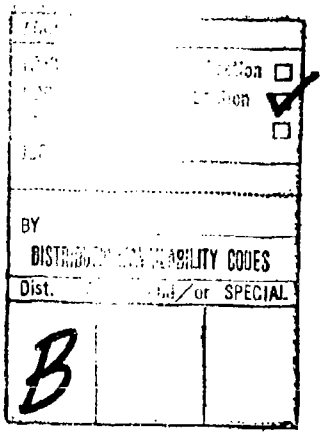

(U) TABLE OF CONTENTS

		Page No.
1.	INTRODUCTION	1
2.	THE BEAM NOISE TIME SERIES	2
	2.1 The Total Beam Power	3
	2.2 The Spectral Line and the Background Components	7
3.	IMPLICATIONS FOR TARCET DETECTION AND CLUTTER	15
4.	INTERPRETATION OF THE BEAM NOISE IN TERMS OF THE SHIPPING DISTRIBUTION	24
5.	SUMMARY	25
6.	ACKNOWLEDGEMENTS	26
7.	REFERENCES	26
APPENDIX A -	Experiment and Data Processing Background	27
APPENDIX B -	The Decomposition Algorithm	29
APPENDIX C -	An Algorithm for Reducing the Effect of Missing Hydrophones	38
DISTRIBUTION		45

List of Illustrations

Figure Number			Page No.
(C)	2.1	Beam Power, MF band, sample one (U)	5
(C)	2,1	Beam Power, HF band, sample one (U)	6
(C)	2.3	Beam Power, MF band, sample two (U)	8
(C)	2.4	Beam Power, HF band, sample two (U)	9
(C)	2.5	Spectral Line Component, MF band, sample one (U)	11
(C)	2.6	Spectral Line Component, MF band, sample two (U)	12
(C)	2.7	Background Component, MF band, sample one (U)	13
(C)	2.8	Background Component, MF band, sample two (U)	14
(C)	2.9	Spectral Line Component, HF band, sample one (U)	16
(C)	2.10	Background Component, HF band, sample one (U)	17
(C)	3.1	SB1B Component, MF band, sample one (U)	14
(C)	3.2	SB1B Component, MF band, sample two (U)	20
(C)	3.3	SB1B Component, HF band, sample one (U)	21
(C)	3.4	Number of spectral lines vs threshold constant(U)	23
(C)	B.1	Spectral Line Component; Azimuth smoothing only(U)	35
(C)	B.2	Background Component; Azimuth smoothing only (U)	36
(C)	B.3	Spectral Line Component; Both azimuth and frequency smoothing (U)	37
(C)	C.1	Beam power obtained using only hydrophones present (U)	42
(C)	C.2	Beam power obtained using estimates for missing hydrophones (U)	43

List of Illustrations (cont'd)

Figure Number			Page No.
(C)	C.3	Azimuthal Power Distributions at 280 Hz (U)	44
(C)	C.4	Azimuthal Power Distributions at 276.6 Hz (U)	45

LIST OF TABLES

(S)	A.1	Beamwidths (3dB) (U)	27

This Page Intentionally Blank

PRELIMINARY RESULTS OF AN ANALYSIS OF BEAM NOISE IN THE MEDITERRANEAN(U)

1. INTRODUCTION

(S) The beam noise measured on the LAMBDA II array system during Task V of the Mediterranean ASW Augmentation Program is currently being analyzed in two 30 Hz frequency bands: a 275-305 Hz band, measured on the high frequency (HF) array segment, and a 30-60 Hz band, measured on the medium frequency (MF) array segment. This report presents preliminary results, obtained at an intermediate stage of the analysis, along with a description of the methodology and the processing algorithms.

(C) The objective of the analysis is to statistically characterize the narrowband/narrowbeam noise over broad regions of the frequency-azimuth plane. To this end, the total beam power is decomposed into two components: a spectral line component, which consists of the narrowband lines which are resolved in frequency, and a background component, which consists of the total contribution from those sources which are not resolved in frequency and may or may not be resolved in azimuth. The spectral line component determines the false target environment against which target classification algorithms must operate. This component will be characterized in terms of the probability distributions of the number of lines in specific regions of the frequency-azimuth plane along with the distributions of the spectral line power in these regions. The background component determines the minimum level that a narrowband line must exceed in order to be detected. This component, together with the total beam noise, will be characterized in terms of probability distributions computed as functions of both frequency and azimuth. The results of this analysis will provide a statistical basis for evaluating the surveillance capability of systems with frequency and azimuth resolution characteristics similar to the LAMBDA II, MF and HF array segments in high shipping density regions such as the Ionian Basin.

(S) The preliminary results in this report are based on the time series of the frequency-azimuth distribution of the total beam power and its spectral line and background components. The characteristics of these time series are illustrated in Section 2 in terms of two samples from both the 30-60 Hz, MF band and the 275-305 Hz

Note: Manuscript submitted July 14, 1978.

(S) HF band. In Sections 3 and 4, these characteristics are interpreted in the light of a shipping density estimate taken during the observation period and their implications on target detection and clutter are discussed. The processing algorithms, including the procedure used to reduce the effect of the missing hydrophones on the beam pattern sidelobe structure, are discussed in the Appendices.

(S) The preliminary results to date are as follows:

The beam noise in the HF band, as well as the MF band, is primarily due to shipping.

The azimuthal variation in the beam noise in both bands is in qualitative agreement with shipping survey data.

Different noise sources contribute to each band, indicating that at least two (acoustic) classes of ships are present.

The observed results in the HF band, together with the results of ref [1], suggest that the 300 Hz line of a Type II target should be visible in an essentially clutter free environment approximately 50% of the time

The 50 Hz line of a Type II target should rarely be visible in the MF band in a low clutter environment.

The error in the beam noise estimates induced by the three missing hydrophones in the HF array segment can be reduced significantly with a simple modification to the beamforming algorithm.

2. THE BEAM NOISE TIME SERIES

(C) The beam noise in the 30-60 Hz, MF band is highly anisotropic with individual samples exhibiting broadband components consisting of both the narrowband lines and the frequency continuous contributions from the noise source field.* Furthermore, the extent of the anisotropy varies considerably with time. During approximately two-thirds of the time series, a few strong noise sources dominate the beam noise, causing significantly larger azimuthal variations than during the rest of the time series when no dominate noise source are evident

*In this report, the term "broadband component" refers to a concentration of beam power across the frequency band at a given azimuth. The term "frequency-continuous" refers to that constituent that is smooth with respect to frequency.

(C) The beam noise in the 275-305 Hz, HF band is similar in character to that in MF band but differs significantly in the extent of the azimuthal variation, the number of narrowband lines and the power in those lines. Furthermore, there is little correlation between the broadband components in the HF band and those in the MF band indicating that the noise sources which dominate in one band are not necessarily dominant in the other.

(U) To illustrate these characteristics, two samples from each frequency band have been selected from the time series. The first sample is chosen from a period when the noise in the MF band is dominated by two broadband components while the noise in the HF band has several relatively small broadband components. This sample is fairly typical of the majority of both the MF and HF time series. The second sample is chosen from a period when there are no dominant braodband components in the MF band but several relatively large broadband components in the HF band. This sample, although less typical than the first, illustrates the extent of variation in the time series.

2.1 The Total Beam Power

(S) The time series of the beam noise were obtained over a forty-three hour period during which the LAMBDA II system was towed over short, east-west tracks in the southern part of the Ionian Basin. During this period, a source transmitting cw signals at 280 and 40 Hz with source levels of 173 and 150 dB//uPa, was towed in an easterly direction. The beam power was computed using a 10 minute average (21 time samples), at .2 Hz intervals in both the MF and HF frequency bands. The broadside beamwidth at the highest frequency in each band is approximately 2.6 degrees; this value increases by a factor of two over the MF band, but only by a factor of 1.1 over the HF band. Additional details can be found in Appendix A and reference [1].

(C) The first samples of the total beam power are illustrated in Figures 2.1 and 2.2 in an intensity-modulated format. In these plots, eight shades are used to represent a 24 dB range in 4 dB increments with increasing shade darkness corresponding to increasing beam power. The black shade represents beam powers in excess of the 78 dB maximum and the white shade represents values below the 54 dB minimum. All values are relative to the intensity

(C) of a luPa planewave measured at the hydrophone inputs.* The frequency axis, which spans the 30 Hz range for each band, has tic marks separated by 1.76 Hz. The azimuth axis is linear in the sine of the azimuth variable with zero degrees corresponding to due north.**

(C) The total beam power in the MF band, Figure 2.1, is dominated by two broadband components at approximately -30 deg. and -3 deg. These components yield variations with azimuth of up to 34 dB depending on frequency. An examination of these components at the higher frequencies (narrower beamwidths), suggests that each component is due to more than one noise source. This is born out in the time series in the vicinity of the sample which shows that each component is primarily due to two sources moving in opposite directions. Also evident in Figure 2.1 is a harmonic component at -75 degrees with lines spaced approximately 6.5 Hz apart and a smaller component at 40 degrees which has a peak in its spectrum at approximately 46 Hz. The weak component at 90 degrees may be due to noise radiated from the array tow ship.

(C) The plot of the beam noise in the HF band, Figure 2.2, shows a very strong broadband component, several lesser components and two weak components in addition to the 280 Hz signal line. The strong component at 70 degrees and the intermediate component at 10 degrees can be attributed to array tow ship noise, with the strong component due to the direct path arrival and the intermediate component due to arrivals which have been reflected from the bottom and the surface. This hypothesis is support by the fact that both these components are present throughout the time series at the same azimuths relative to forward endfire, regardless of the tow ship heading. Furthermore, the arrival directions associated with these azimuths are consistent with the location of the array relative to the array tow ship and the bottom.

(U) The remaining broadband components, which exhibit azimuthal variations of the order of 10 dB or less, can be attributed to sources

---

*The beam values are obtained by subtracting the theoretical signal gain (30.dB) from the observed values. Alternatively, the beam power can be referred to an uncorrelated noise field by adding 25.95 dB which represents the sum of the theoretical array gain (18.75 dB) and a bandwidth correction factor of 5.2 dB.

**The array headings for the first and second samples were 90 degrees and 89 degrees respectively.

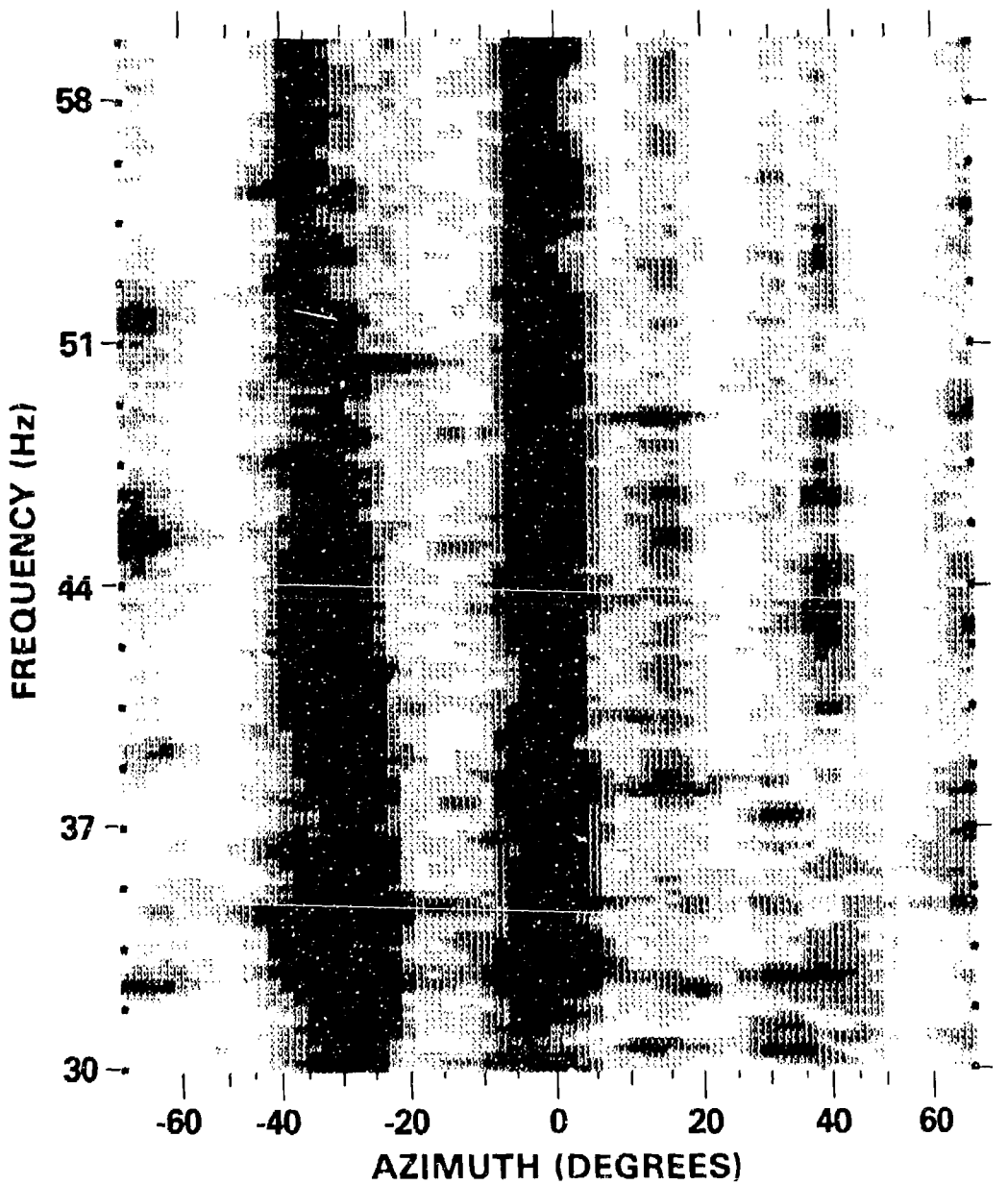

Fig. 2.1 (C) — Beam power, MF band, sample one;
54-78 dB//uPa; 16 Nov. 74, 1110Z (U)

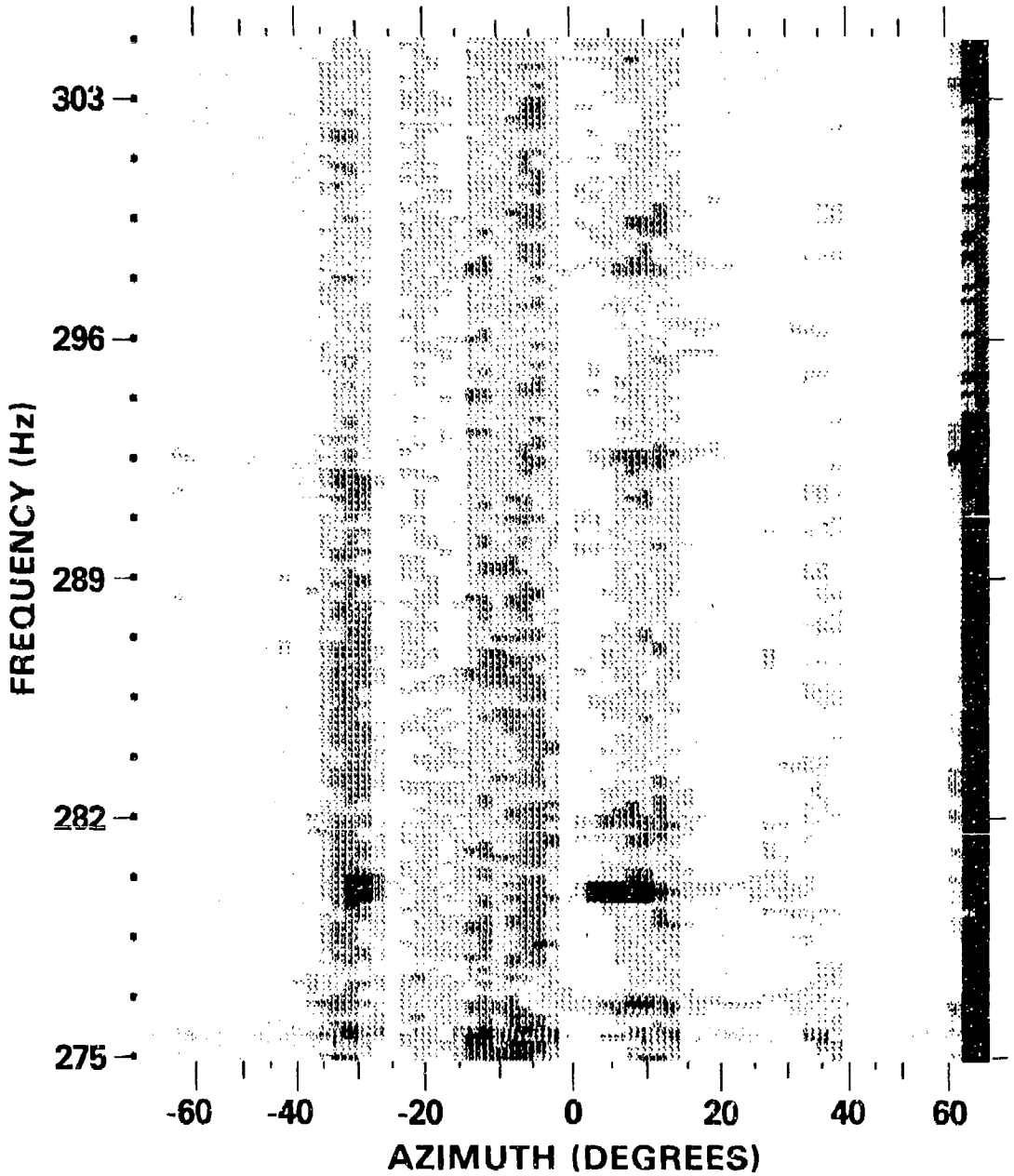

Fig. 2.2 (C) — Beam power, HF band, sample one;
42-66 dB//uPa; 16 Nov. 74, 1050Z (U)

(U) other than the array tow ship. The three components at -30, -5 and 38 degrees have counterparts in the MF noise of Figure 2.1 which was measured 20 minutes later, and thus, could possibly be due to the same noise sources. The remaining components, however, have no counterparts in the MF band.

(U) Finally it is noted that there are two low noise directions in the vicinity of 50 degrees on either side of zero azimuth. This is typical of much of the time series for both the MF and HF bands and is consistent with the shipping survey data which shows that most of the ships are concentrated in a 100 degree sector about zero degrees.

(U) The second sample from the MF band, measured approximately 20 hours after the first, is plotted in Figure 2.3. In contrast to the first sample, there are only a few instances where the beam noise exceeds the 78 dB upper limit of the plot and the azimuthal variations are typically of the order of 12 to 16 dB. The broadband components, which span much larger azimuthal sectors than those in sample one, can be attributed to the contributions from many sources, none of which dominate. The comparatively low levels in this sample are typical of the latter one-third of the time series.*

(C) The second sample from the HF band, measured 12 minutes after the second MF sample, is plotted in Figure 2.4. In this sample, there are five broadband components in addition to the two components due to the array tow ship noise and the 280 Hz signal line. In contrast to the first sample, these components are not restricted to 50 degrees on either side of zero azimuth and they show a somewhat larger azimuthal variation. Furthermore, three of these components, at -70, 25 and 45 degrees, occur at azimuths where there are no counterparts in the second MF sample. Finally, it is noted that the beam levels due to the array tow ship noise are generally higher than those in the first sample. This increase is particularly evident in the reflection of a 285 Hz spectral line appearing at 10 degrees azimuth.

2.2 The Spectral Line and the Background Components

(U) The background component represents an estimate of the frequency continuous portion of the total beam power. The spectral line component consists of those narrowband lines which exceed the background by at least 2.6 dB. The two components are computed so that they sum in a linear scale to yield the total beam power. As a result, each component can be interpreted as the total power, given that the other

*These comparatively low levels might be due to reduced shipping activity, since the latter one-third of the time series occurred on a Sunday morning.

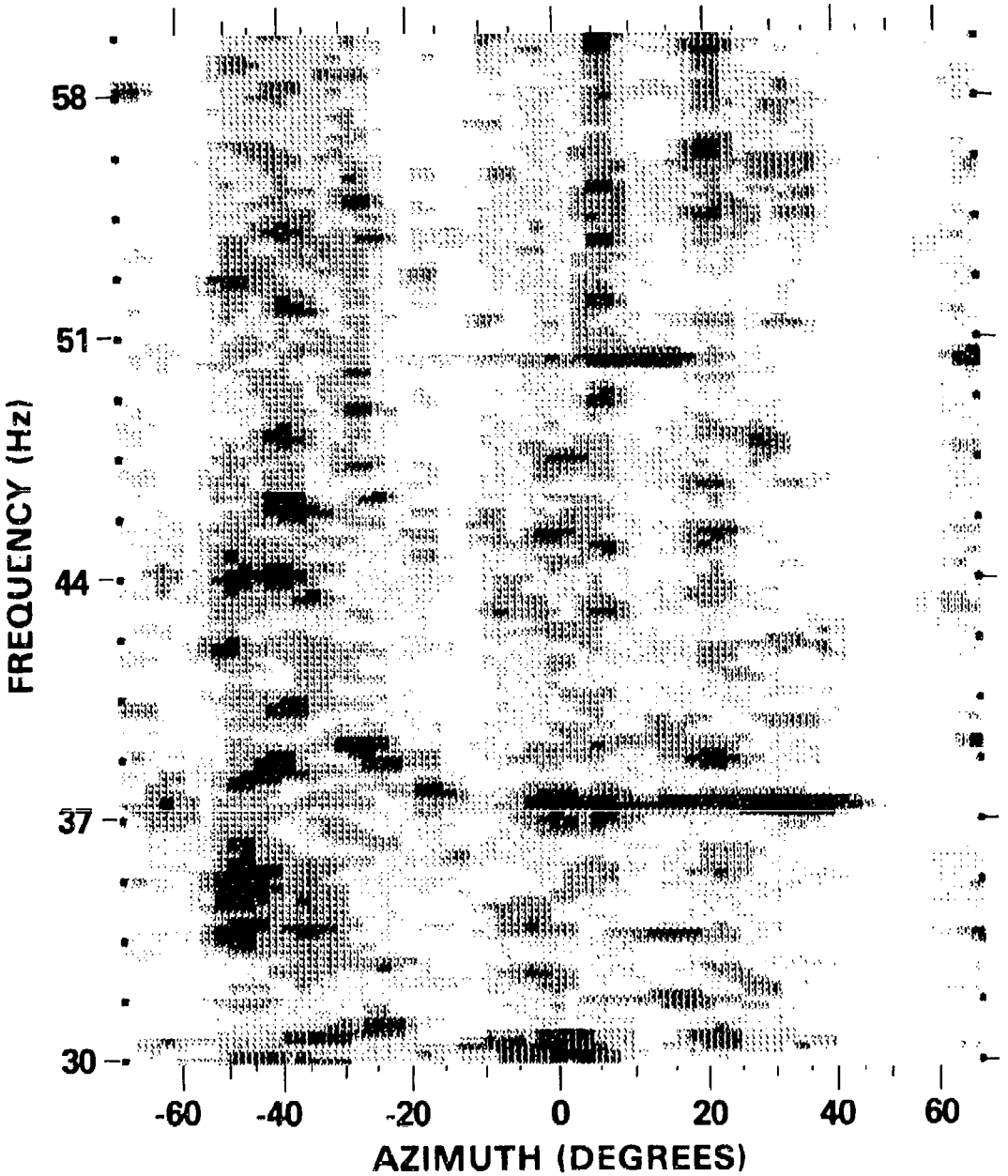

Fig. 2.3 (C) — Beam power, MF band, sample two
54-78 dB//uPa; 17 Nov. 74, 0640Z (U)

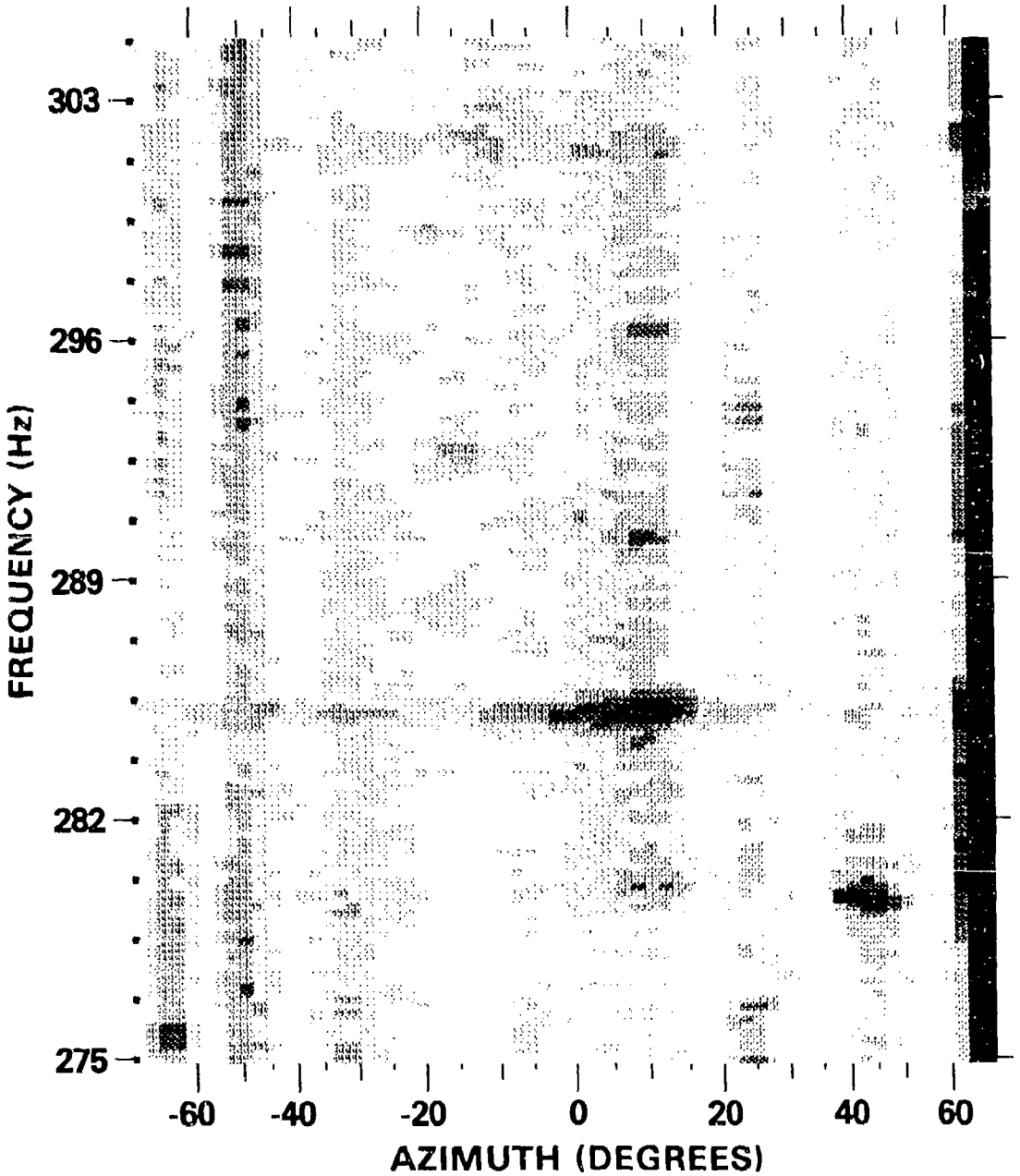

Fig. 2.4 (C) — Beam power, HF band, sample two
42-66 dB//uPa; 17 Nov. 74, 0652Z (U)

(U) component were zero. The threshold constant of 2.6 dB was chosen to limit the probability of detecting a line when none is present to .004. The algorithm used to decomposed the total beam power into its spectral line and background components is described in detail in Appendix B.

(U) The spectral line component for the first sample in the MF band is plotted in Figure 2.5. The format is similar to that of the preceding section except that the dynamic range spans only 18 dB in 3 dB steps, and the frequency range is reduced by 3.1 Hz due to end effects in the decomposition algorithm. The spectral lines associated with the broadband components identified in the total beam power, are clearly evident. The harmonic structure associated with these lines is consistent with a fundamental frequency corresponding to either the blade rate or the shaft rate of merchant ships. In addition, other lines appear in Figure 2.5 which do not appear in Figure 2.1 due to the 4 dB step size. The power in the spectral lines ranges from 56 dB up to as much as 85 dB for some of the lines associated with the dominant broadband components in the total power.

(U) The spectral line component for the second sample in the MF band is plotted in Figure 2.6. The power in the spectral lines for this sample is significantly less than for sample one since there are no dominant broadband components in the total beam power. On the other hand, a detailed examination of Figures 2.5 and 2.6, shows that the number of distinct spectral lines in both samples is approximately the same; 258 in the first sample and 260 in the second. These results suggest that, for threshold constants of the order of 2.6 dB, the number of detected spectral lines should be relatively independent of the distribution of the spectral line power.

(U) The background components for both samples in the MF band are plotted in Figures 2.7 and 2.8. The frequency-continous spectra associated with the broadband components in the total power are evident in both the background components. The two large broadband components which dominate the total power in the first sample, yield azimuthal variations of up to 25 dB in the corresponding background component of Figure 2.7. In contrast, the azimuthal variation in the background component of Figure 2.8 seldom exceeds 15 dB. Furthermore, at the azimuths where the spectrum level is large, there is more variation with frequency evident in Figure 2.7 than in Figure 2.8. This can be attributed to the fact that the background component for sample two, to a greater extent than sample one, represents the contributions from many noise sources so that the frequency characteristics of individual sources are less apparent.

(U) The plots of the spectral line component and the background component for sample one in the HF band are shown in Figures 2.9 and

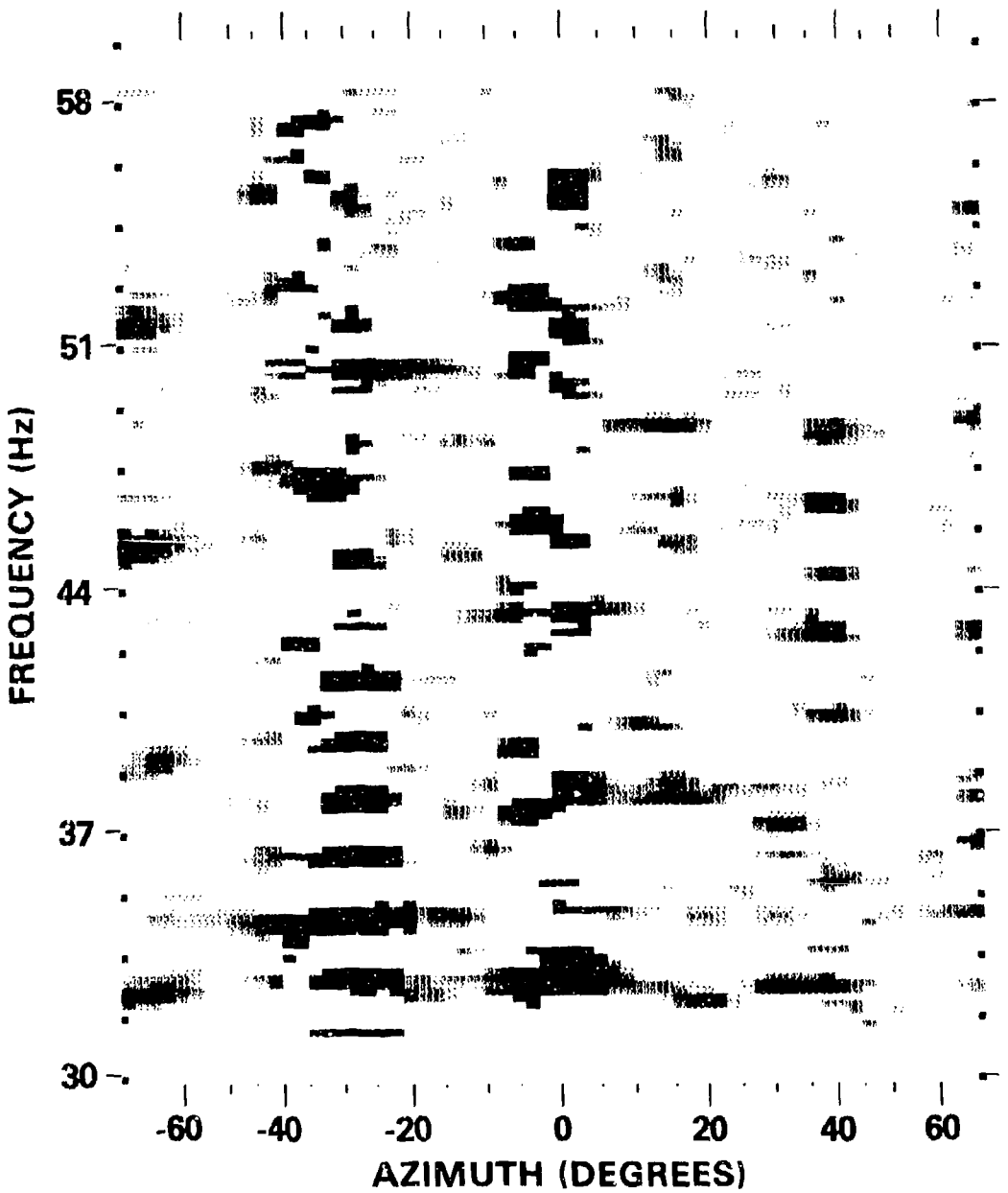

Fig. 2.5 (C) — Spectral line component, MF band, sample one
56-74 dB//uPa; 16 Nov. 74, 1110Z (U)

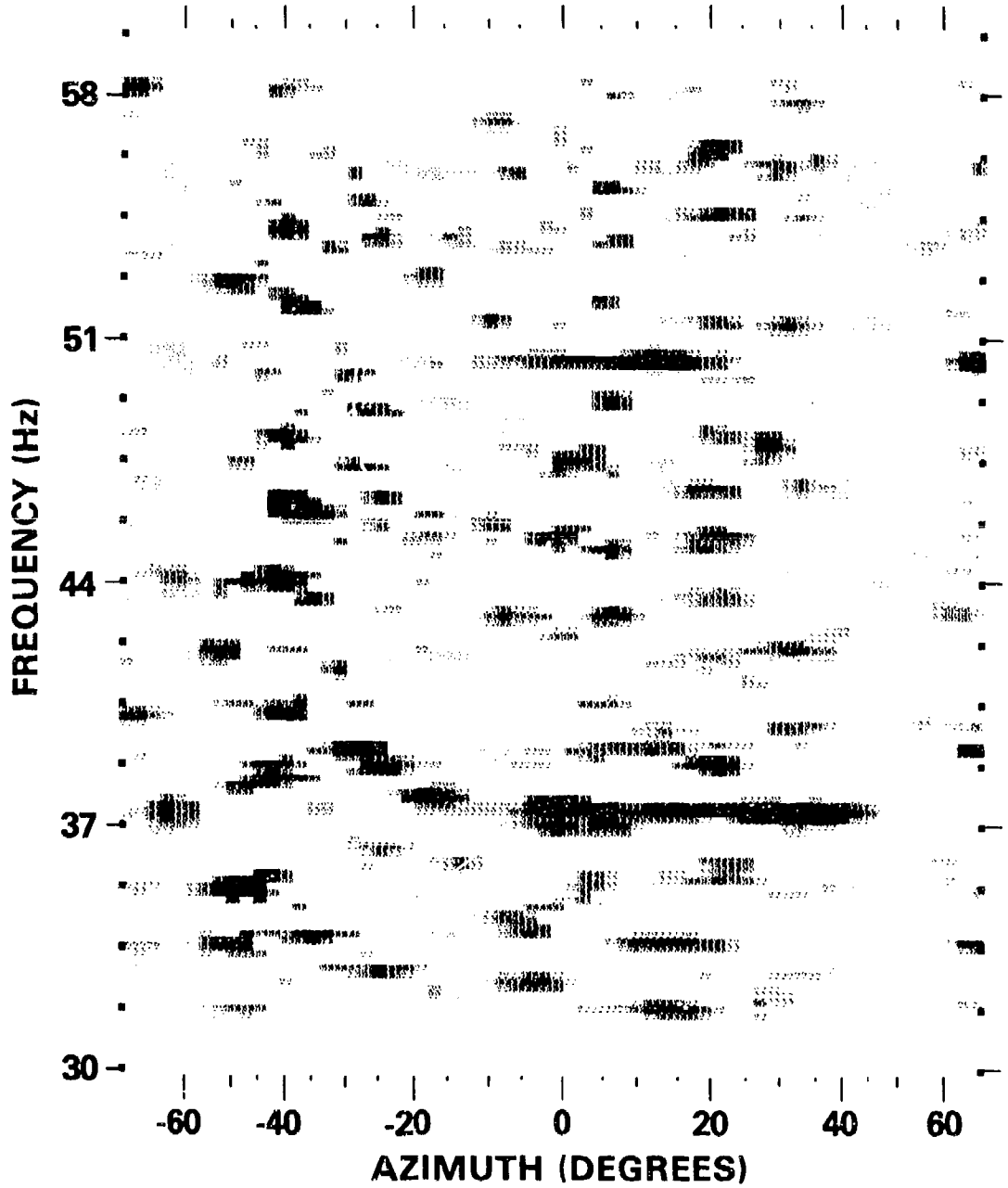

Fig. 2.6 (C) — Spectral line component, MF band, sample two
56-74 dB//uPa; 17 Nov. 74, 0640Z (U)

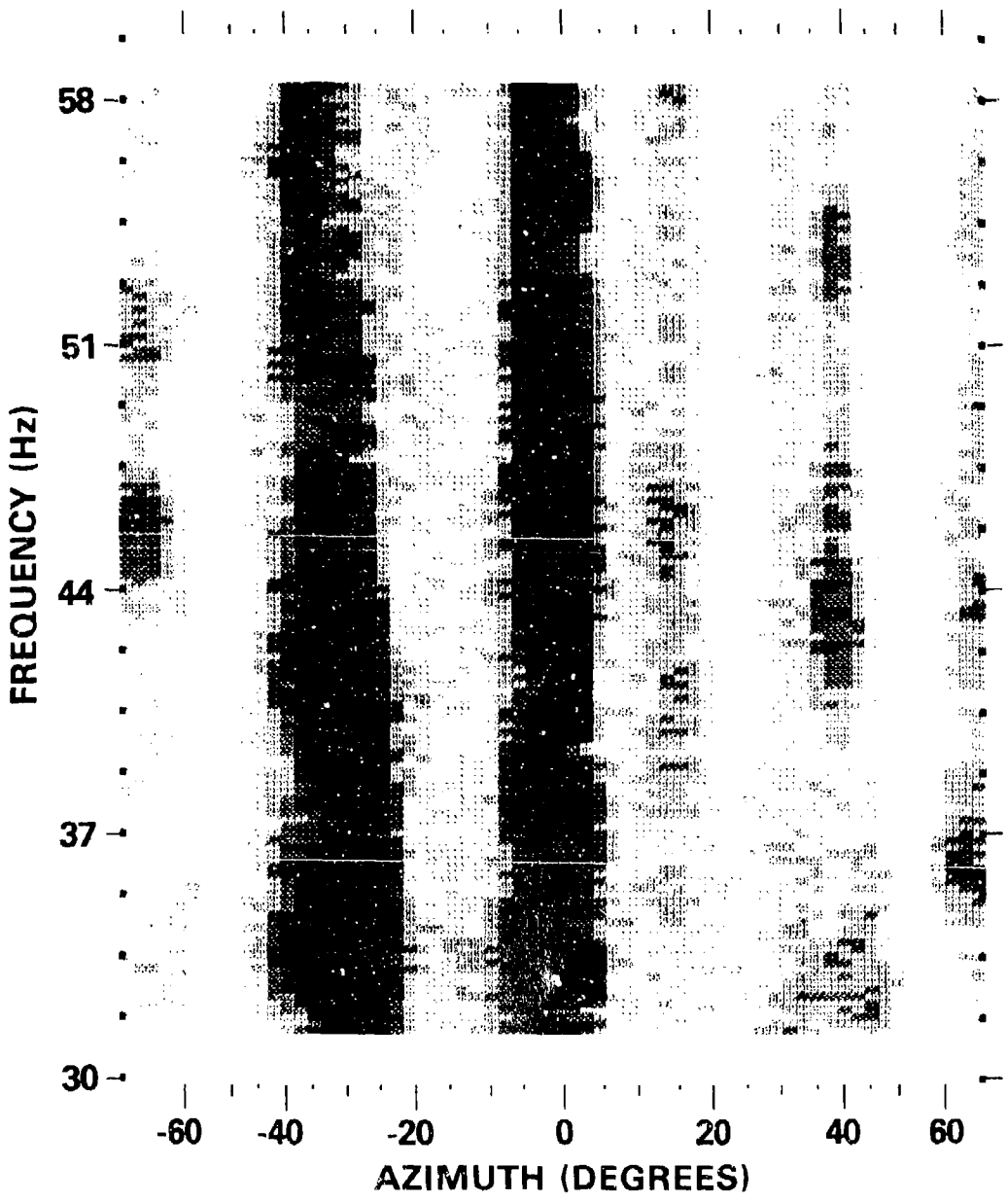

Fig. 2.7 (C) - Background component, MF band, sample one
56-74 dB//uPa; 16 Nov. 74, 1110Z (U)

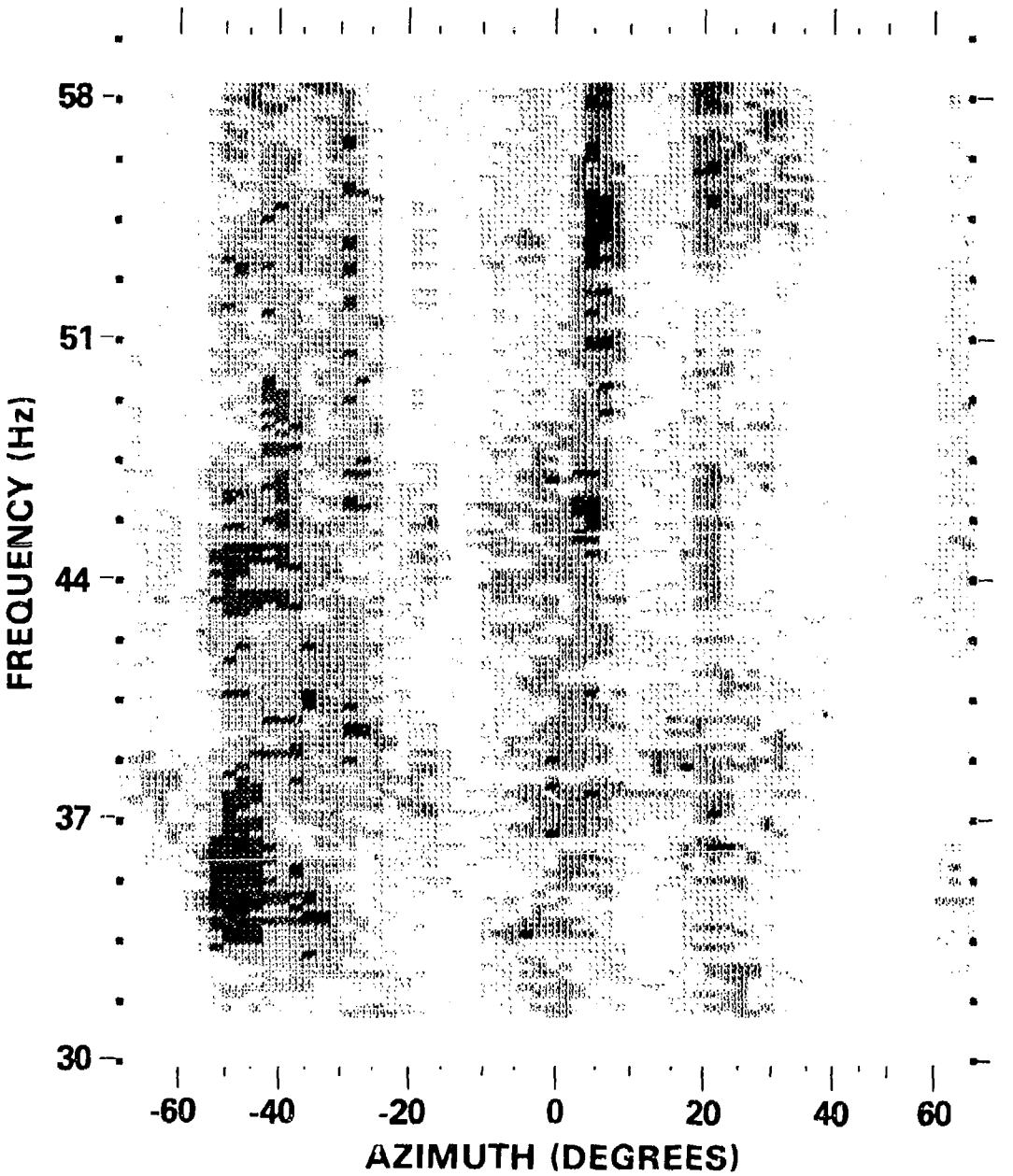

Fig. 2.8 (C) — Background component, MF band, sample two
56 71 dB//uPa; 17 Nov. 74, 0640Z (U)

(U) 2.10 respectively. The narrowband lines associated with the direct and the reflected arrivals of the array tow ship noise appear at 70 and 10 degrees in Figure 2.9 and the frequency-continuous contributions appear at the same azimuths in Figure 2.10. A comparison of Figure 2.9 with Figures 2.4 and 2.5 shows that there are fewer spectral lines in the HF band than in the MF band.* In particular, excluding the lines associated with the array tow ship noise and the 280 Hz signal line, there are approximately 175 lines in the HF band as compared with approximately 260 lines in each sample from the MF band. Furthermore, the spectral line power in the HF band shows less variation than in the MF band, with all but a few lines having levels restricted to a 9 dB range between 42 dB and 51 dB.

(U) The background component, Figure 2.10, shows frequency and azimuthal variations that are slightly less than sample two in the MF band and significantly less than sample one. Excluding the component due to the direct arrrival of the array tow ship noise, the largest azimuthal contrast, of about 15 dB, occurs between the low noise direction at -50 degrees and the broadband component at -30 degrees. For azimuths within + 50 degrees, which excludes the low noise direction, the beam levels vary by less than 10 dB at all frequencies.

(U) It is important to note that at no azimuths can the beam level be attributed to wind generated noise alone. For example, if the wind noise is assumed to be spatially and temporally uncorrelated, then an omni-directional spectrum level of 55 dB//uPa, which would correspond to the observed sea state one, would result in a beam noise of 33.5 dB. This level is 6.5 dB lower than the lowest beam level observed in the background component of Figure 2.10.

3. IMPLICATIONS FOR TARGET DETECTIONS AND CLUTTER

(U) A narrowband/narrowbeam surveillance system operates on the beam noise to detect the presence of signal lines and to classify these detections into false target lines and real target lines. Signal lines due to both false targets and real targets are detected when they exceed the background by some threshold constant. An increase in the threshold constant reduces the number of false target lines, but it also reduces the percentage of time that the real target lines are

*As was the case in the MF band, the number of spectral lines in both samples in the HF band is approximately the same; 172 in the first sample and 178 in the second.

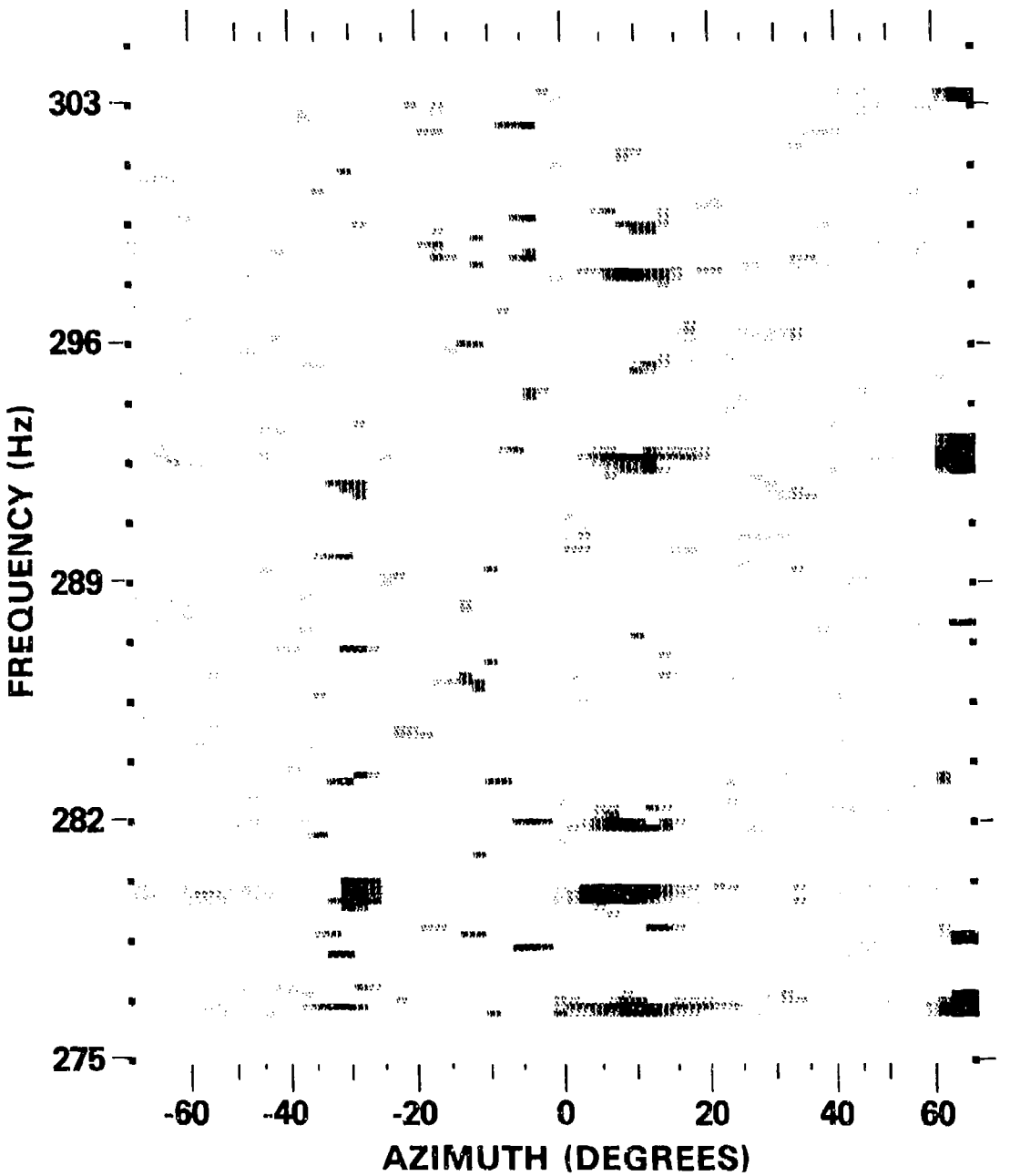

Fig. 2.9 (C) — Spectral line component, HF band, sample one
42-60 dB//uPa; 16 Nov. 74, 1050Z (U)

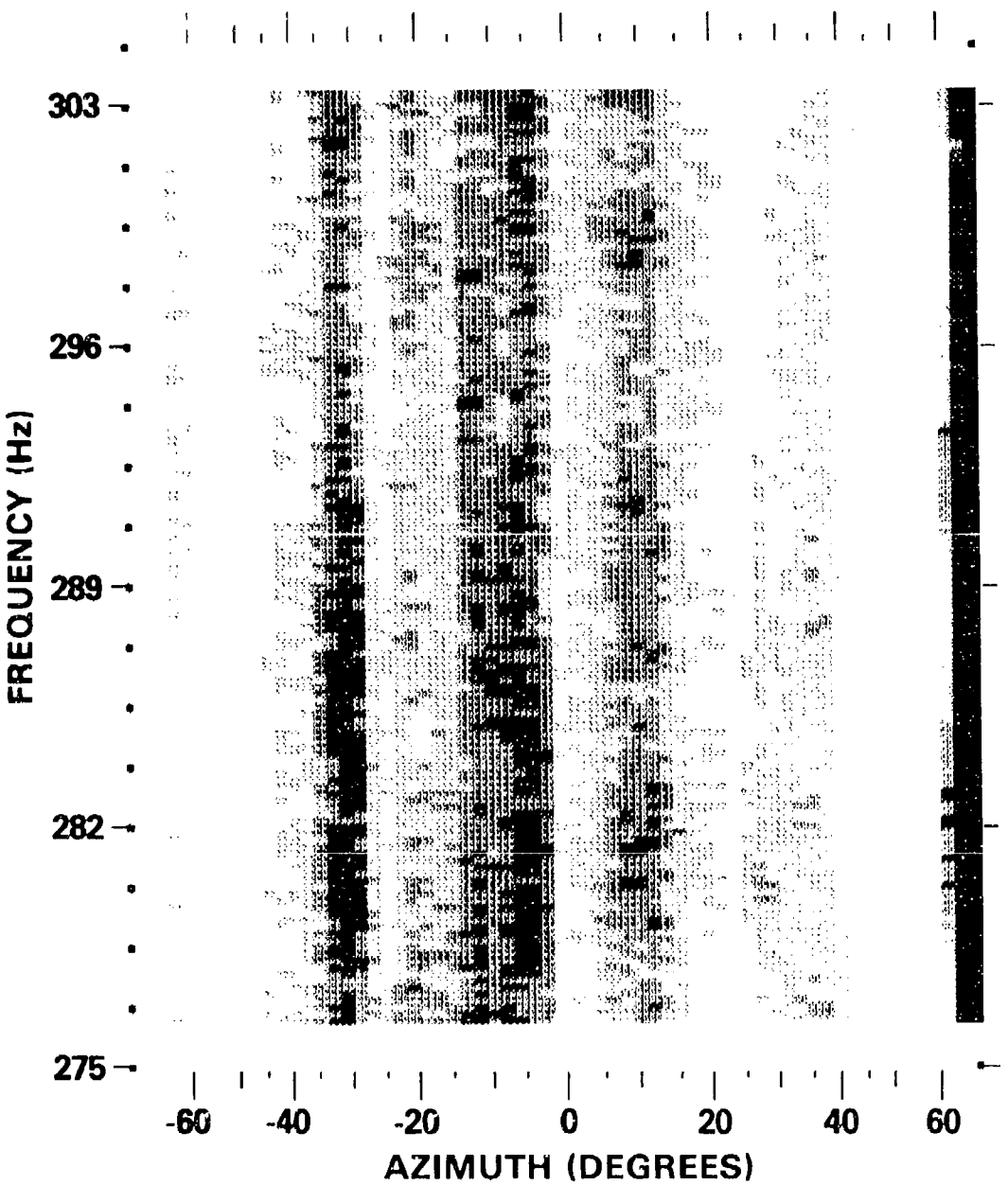

Fig. 2.10 (C) – Background component, HF band, sample one
42-60 dB//uPa; 16 Nov. 74, 1050Z (U)

(U) visible. Thus, the choice of a threshold constant represents a compromise between the extent of the clutter environment, and hence, the magnitude of the classification problem,* and the probability of detecting the real target lines. In this section, the results of Section 2, together with those of reference [1], are used to investigate this compromise.

(U) The dependence of the number of detected lines on the value of the threshold constant can be investigated in terms of the ratio of the total beam power to the background power. Plots of these ratios differ from the plots of the spectral line component in the preceding section in that they sum in a decibel scale with the background component to yield the total power. In the context of "signal" line detections, these ratios represent a "signal-plus-background to background ratio" which is denoted here by** SB/B. The number of spectral lines that are detected using a given threshold constant c, is obtained from the plot of the SB/B component by a count of the number of times SB/B exceeds c.

(U) The SB/B components for both samples in the MF band and the first sample in the HF band are illustrated in Figures 3.1, 3.2, and 3.3. The range of these plots spans 0 to 12 dB in 2 dB steps and values less than 2.5 dB have been deleted so that the only spectral lines that appear are those that appear as spectral lines in Section 2.

(U) A comparison of the SB/B components for the two samples in the MF band, Figures 3.1 and 3.2, shows that even though the power in the spectral line component for sample one is significantly larger than for sample two, the SB/B ratios are approximately the same. This can be attributed to the fact that an increase in the spectral line power is accompanied by an increase in the background component due to an increase in the frequency-continuous portion of the spectrum from the dominant sources.

(U) In the plot of the SB/B component for the HF band, Figure 3.3, it is seen that the SB/B ratios are distributed over a smaller range than those in the MF band. As a consequence, small increases in the

---

*The classification of the spectral lines depends on the difference in the line properties, center frequency, bandwidth, stability etc., between the false target lines and the real target lines.

**The SB/B ratio is related to the signal-to-background ratio, S/B, by

$$SB/B = 10 \log (1 + S/B)$$

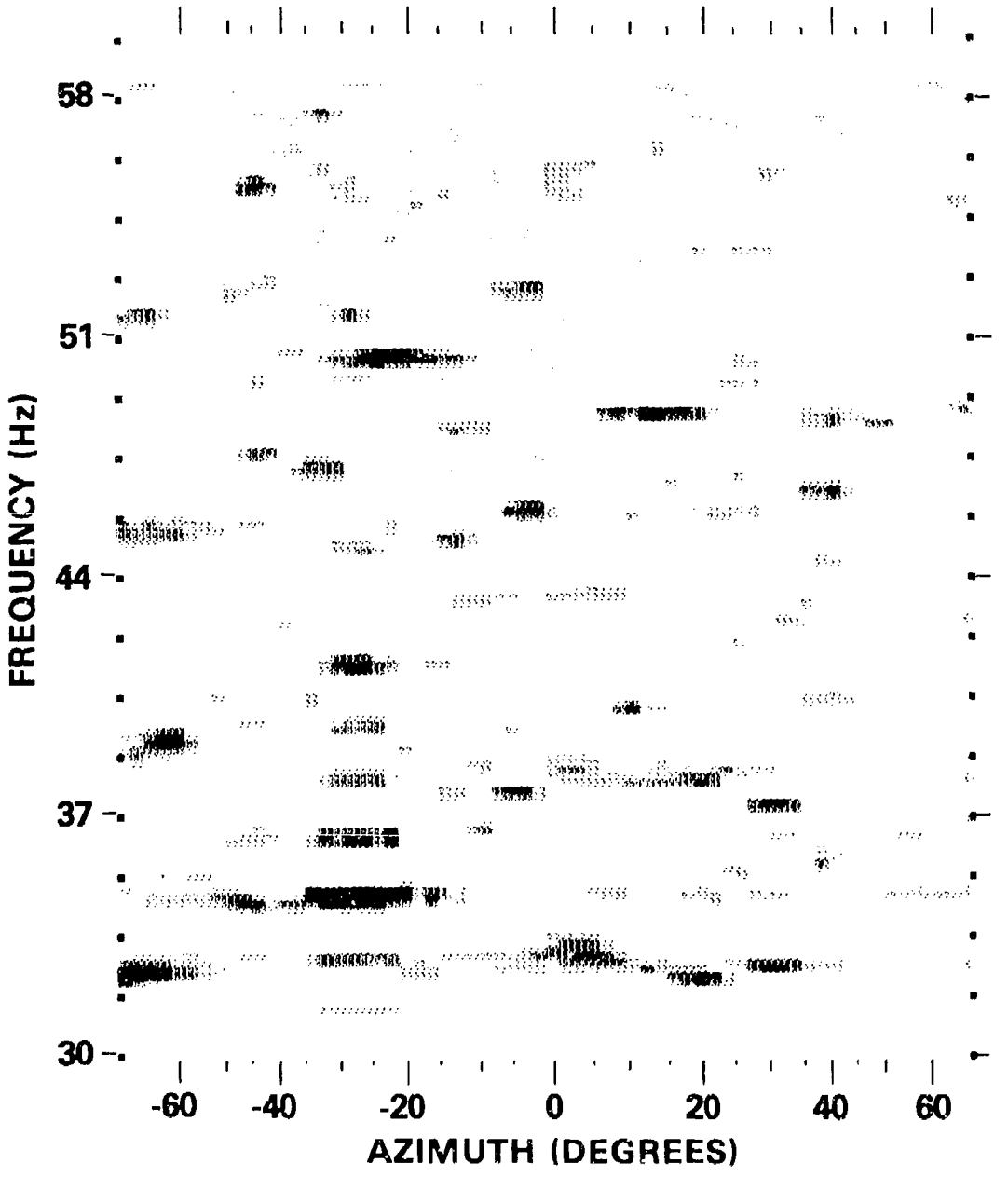

Fig. 3.1 (C) — SB/B component, MF band, sample one
0-12 dB; 16 Nov. 74, 1110Z (U)

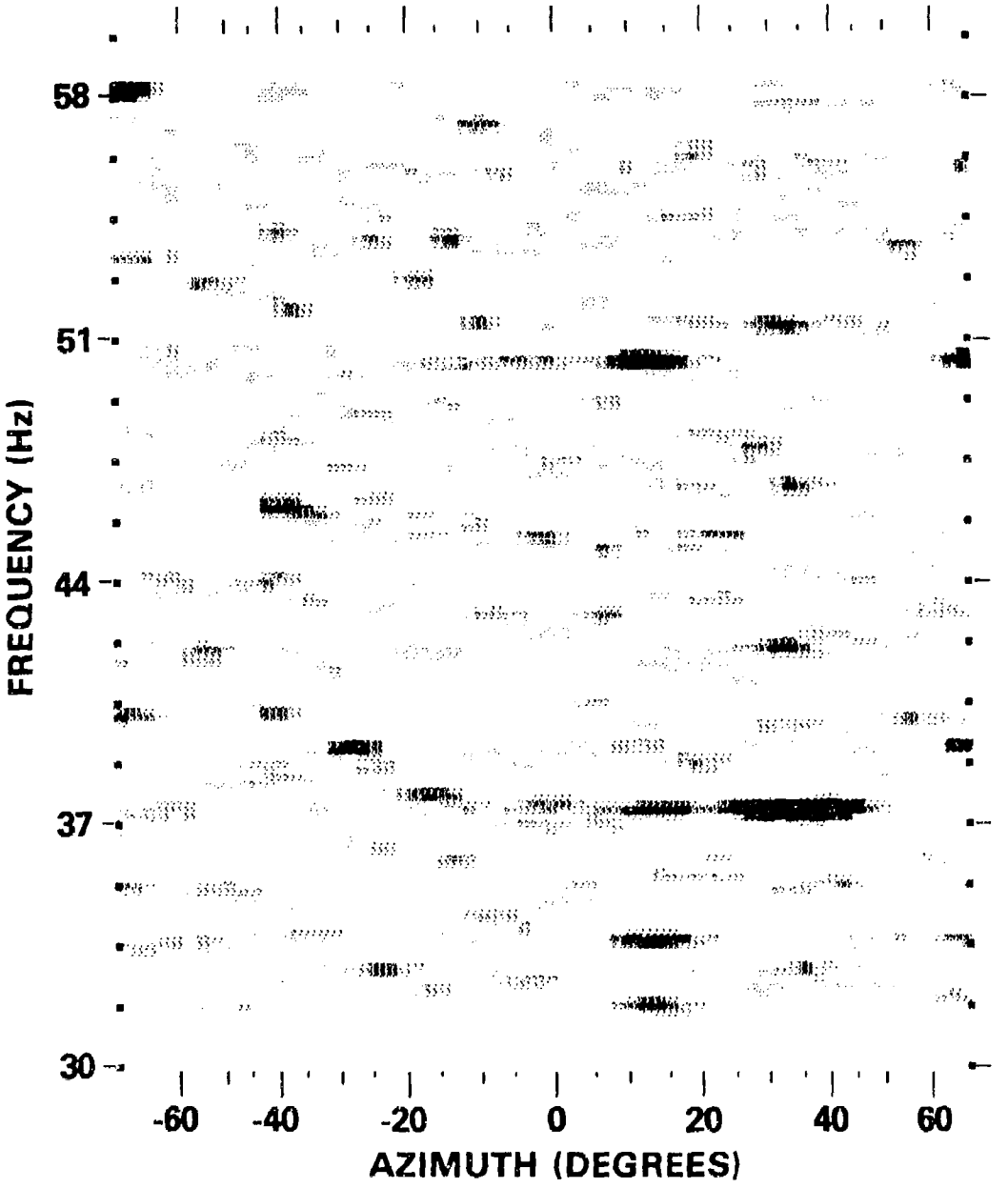

Fig. 3.2 (C) — SB/B component, MF band, sample two
0-12 dB; 17 Nov. 74, 0640Z (U)

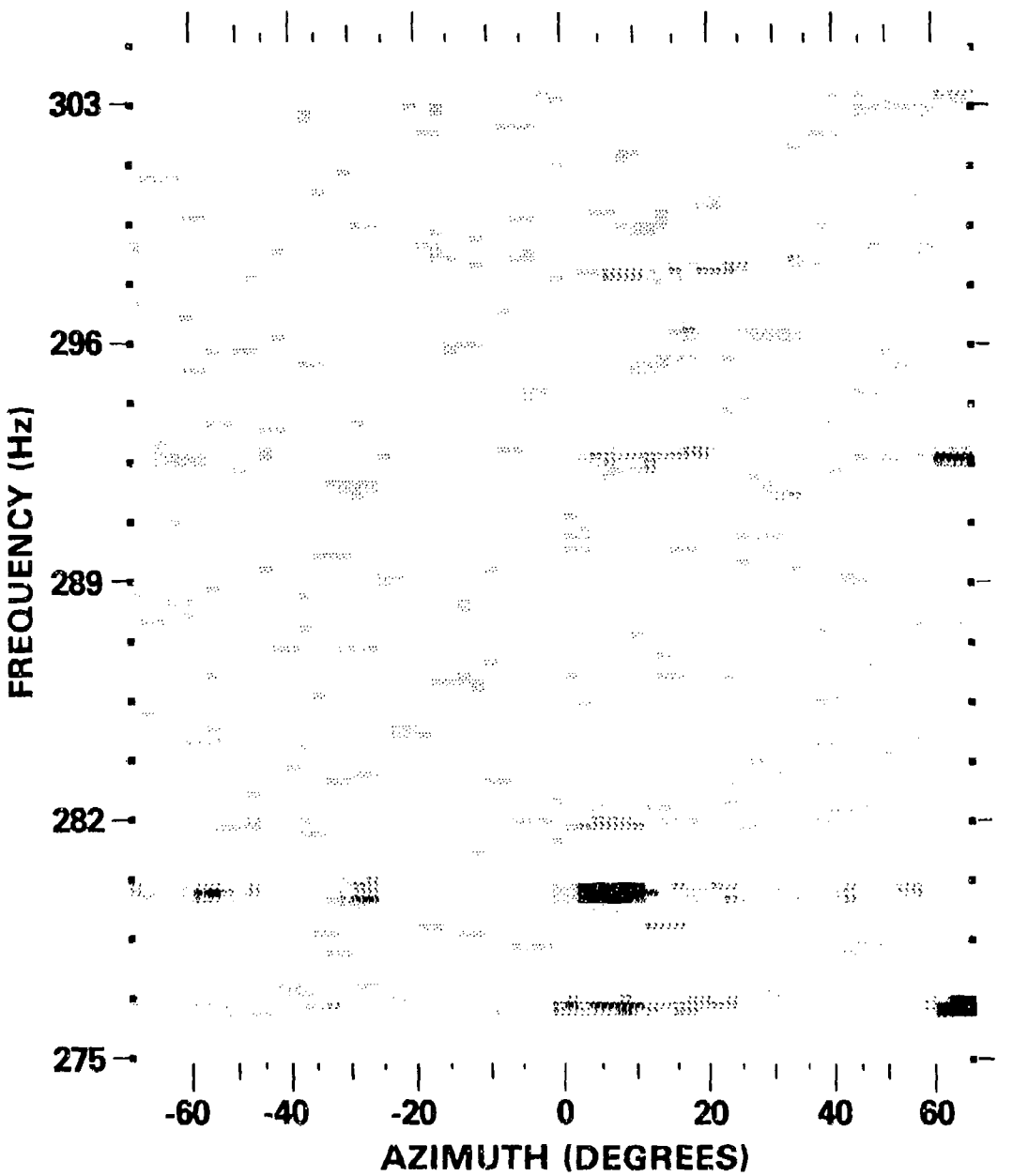

Fig. 3.3 (C) — SB/B component, HF band, sample one
0-12 dB; 16 Nov. 74, 1050Z (U)

(U) threshold constant will have a greater effect on the number of detected lines in the HF band. To illustrate this effect, we have computed the average number of detected lines over both samples in each frequency band for different values of the threshold constant. The results* are plotted in Figure 3.4.

(U) Figure 3.4 shows a dramatic difference in the dependence of the number of detected lines on the value of the threshold constant for the two frequency bands. For example, in the HF band, an increase in the threshold constant from 2.6 to 4 dB, reduces the number of lines by 90 percent, and only one line is detected for a threshold constant of 8 dB. On the other, in the MF band, the increase from 2.5 to 4 dB, reduces the number of lines by only 53 percent and 18 lines are detected with a threshold constant of 8 dB.

(S) Figure 3.4 illustrates how increases in the threshold constant reduce the clutter due to the false target lines. The compromise between the extent of the clutter due to false targets and the percentage of time that the real target lines are visible can be seen by considering two examples: the detection of a 300 Hz line with a mean source level of 150 dB and a 50 Hz line with a mean source level** of 153 dB.

(S) Consider the 300 Hz line first. Figure 4.1, reference [1], shows the probability distribution of the 280 Hz, signal-to-noise ratio observed during the experiment. From this Figure, and the discussion of Section 5.0, ref [1], it can be concluded that the 50 percentile of the SB/B ratio for the 300 Hz, target line is approximately 4.75 dB.*** It follows from Figure 3.4, that with a threshold constant of 4 dB, the 300 Hz line will appear as a spectral line in a low clutter environment approximately 50% of the time. On the other hand, it can be seen from Figure 4.1 (ref [1]) and Figure 3.4 that decreasing the threshold constant to 2.5 dB, will greatly increase the clutter without significantly increasing the percentage of time that the 300 Hz line appears.

---

*The number of lines in the HF band does not include the 280 Hz line nor the lines that occur between 5 and 15 degrees and 70 and 90 degrees since at least some of these lines can be attributed to the array tow ship noise.

**These source levels are typical of a Type II target

***The value of 4.75 dB was obtained by equating S/N with S/B, subtracting 23 dB to account for the difference in source levels and adding .97 dB to account for the difference in the analysis bandwidth.

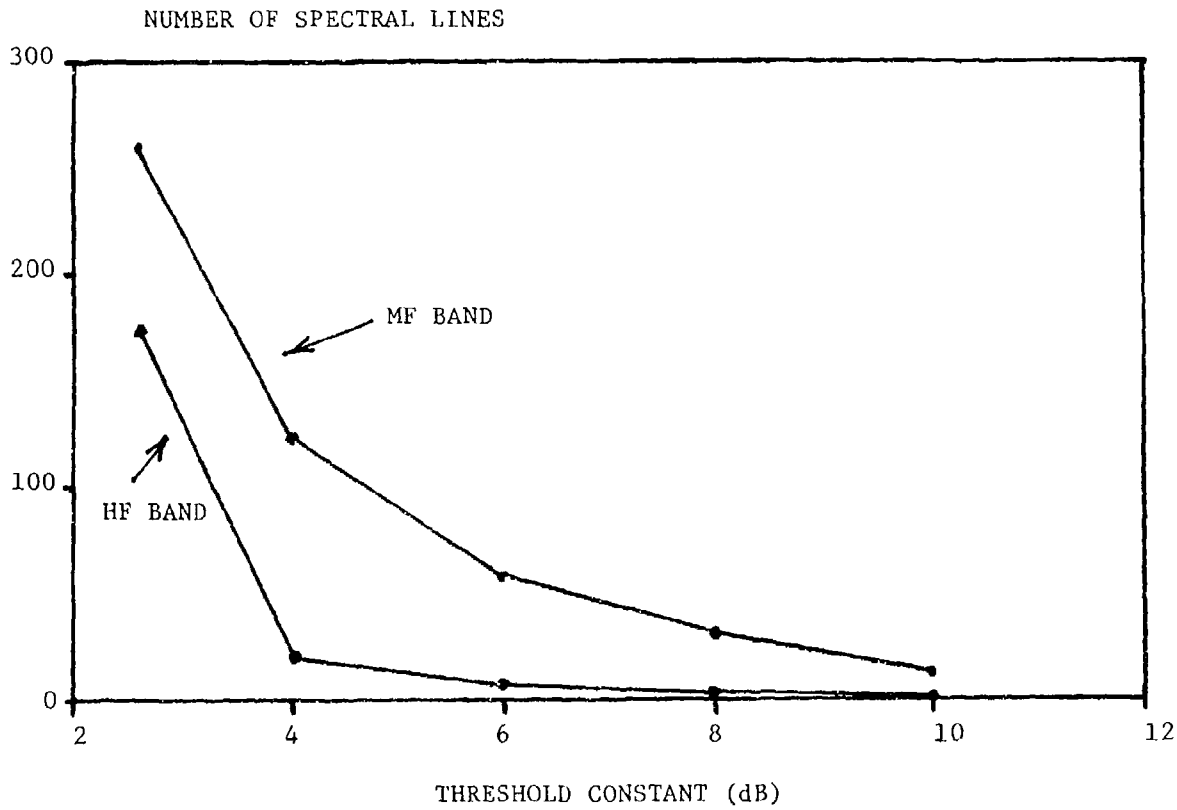

Fig. 3.4 (C) — Number of spectral lines vs. threshold constant (U)

(S) The same analysis cannot be applied to the 50 Hz line, since the signal-to-noise ratio was not measured during TASK V due to the low source level at 40 Hz. It was noted in reference [1], however, and confirmed in this analysis, that the 40 Hz signal line is only rarely visible above the background in the MF band. Since the 40 Hz source level is only several dB lower than that expected from the 50 Hz line, we may conclude from Table 3.1 that detections of the 50 Hz line must occur in a high clutter environment.

4. INTERPRETATION OF THE BEAM NOISE IN TERMS OF THE SHIPPING DISTRIBUTION

(U) The azimuthal variation observed in the beam noise is in qualitative agreement with a sample of the shipping distribution taken during the 43 hour observation period. This sample, Figure 2 of reference [2], shows 211 ships in the Ionian Basin during the period when the first samples from the MF and the HF frequency bands were selected. Of these 211 ships, all but 49 are located within a 100 degree sector centered at zero degrees and all but four of the remaining 49 are located in the image of that sector centered at 180 degrees. Thus, the comparatively low beam noise values observed outside of the 100 degrees sector in both frequency bands are not surprising.

(U) The shipping distribution within the 100 degree sector includes a rather broad shipping lane that traverses the Ionian Basin approximately 250 miles north of the array tow site, plus a concentration of ships along the southeastern coasts of Sicily and Italy, 300 miles to the northeast. These ships are sufficiently dense in azimuth so that several appear on each beam within the 100 degree sector. It is the noise from these ships, both narrowband and frequency-continuous, that probably accounts for much of the noise in the background component.

(U) In addition to these concentrations, the shipping sample shows a scattering of ships which place several within 75 miles of the array tow site. It is these nearby ships which may be the sources of the dominant broadband components which appear in the beam noise in the MF band and to a lesser extent in the HF band.

(C) The interpretation in the preceding paragraphs is necessarily qualitative since the shipping survey did not provide any information from which to infer the source level characteristics of the ships. The need for this information was seen in the samples of the beam noise which showed that many of the broadband components that are significant in one frequency band do not appear in the other frequency band. This result suggests that the ships must be divided into at least two

(C) classes, those which radiate noise primarily at the higher frequencies, such as fishing vessels, and those which radiate primarily at the lower frequencies, such as merchant ships. Thus, without knowing the spatial distribution of each class of ships, the prediction of beam noise statistics using a shipping noise model must be viewed as highly speculative.

5. SUMMARY

(U) The beam noise in the MF band is highly anisotropic with individual samples exhibiting broadband components consisting of both the narrowband lines and the frequency-continuous contributions from the noise source field. The power in both the spectral lines and the background component varies considerably over the 43 hour observation period. However, the number of spectral lines and the signal-to-background ratios for those lines are relatively stable.

(S) The beam noise in the HF band is similar in character to that in the MF band, differing primarily in the extent of the azimuthal variation, the number of spectral lines, the power in those lines, and the relative contribution of the noise generated by the array tow ship. The number of spectral lines in the HF band is approximately 70 percent of that in the MF band with a threshold constant of 2.6 dB. However, both the power and the signal-to-background ratios of these lines are distributed over a much smaller range. As a consequence, the extent of the line clutter due to false targets is a much more sensitive function of the threshold constant in the HF band. This result, together with the probability distribution of the signal-to-noise ratio from reference [1], suggests that the 300 Hz line of a TYPE II target will be visible in a low clutter environment approximately 50 percent of the time, but that the 50 Hz line will almost never be visible in other than a high clutter enviroment.

(C) The beam noise in the HF band, as well as the MF band, is primarily due to shipping, even in the low noise directions, as evidenced by a comparison of the observed beam noise levels with that expected from wind generated noise. The azimuthal variation in the beam noise is in qualitative agreement with that expected from concurrent ship location data which indicates that almost all of the ships are concentrated in a 100 degree sector about due north of the nominal array location and the image of that sector about due south. It was observed, however, that there are many instances where different noise sources contribute in each band, indicating the presence of more than one (acoustic) ship class. As a consequence, the knowledge of the spatial distributions of each of the ship classes may be required for an accurate prediction of the beam noise statistics using shipping noise models.

(U) Finally, in Appendix C, it is shown that if only the hydrophones actually present in the HF array segment are used in beamforming, then large errors in the beam noise can occur at those frequencies where there are strong, spatially coherent signals, such as those due to spectral lines in the array tow ship noise. These errors have been significantly reduced in the results of this report by using an algorithm which forms estimates of the complex amplitudes for each missing hydrophone using the complex amplitudes from the four neighboring hydrophones. This algorithm is described in Appendix C and an example is presented which shows a reduction in the error in the beam noise by as much as 9 dB.

6. ACKNOWLEDGEMENTS

(U) This work was sponsored by the Long Range Acoustic Propagation Project (LRAPP). The authors are particularly grateful to O. Diachok, W. Finney and S. Wales from NRL for the many helpful suggestions during the critical stages of the analysis, to S. Marshall from NORDA who played a major role in the problem definition and to R. Wagstaff from (NOSC) who made the user community aware of the actual hydrophone spacing on the HF array segment.

7. REFERENCES

1. S.W. Marshall, "Acoustic Signal-to-Noise and Azimuthal Noise Directionality in the Mediterranean Sea Using LAMBDA II"(U), NRL Memorandum Report 3050, April 1975 (SECRET).

2. L.P. Soloman and A.E. Barnes, "Summary Report Ionion Basin", TR-004011, Planning Systems Incorporated, McLean, Virginia.

3. W. Finney, "Signal Detection and Estimation in the kw Domain"(U): Presented at the Naval Research Laboratory Signal Processing Workshop, April 1974.

APPENDIX A

Experiment and Data Processing Background

(C) The time series were obtained from off-line computations on recorded hydrophone data during a forty-three hour period from 1530 hours on 15 November to 1030 hours on 17 November 1974. During this period, the LAMBDA II array system was towed at 3 kts by the R/V PACIFIC APOLLO along 18 n.m., east-west tracks, centered at 33° 19' N, 19° 32' E in the Ionian Basin. Simultaneously, a source radiating cw lines at 280 Hz and 40 Hz, with source levels of 73 and 155 dB//uPa, was towed at 6 kts. by the R/V GYRE along an easterly track. The source track and the array tow site are illustrated in the map of Figure 1.1, ref. [1]. During the observation period the source range decreased from 148 to 130 n.m. and then increased to 174 n.m.

(S) The LAMBDA II consists of three, switch-selectable, array segments, only two of which are pertinent to this report. The medium frequency, MF, segment consists of 64, equally-spaced, hydrophone groups yielding an array length of 812 meters and a $\lambda/2$ frequency of 60 Hz. The high frequency, HF, segment is 152 meters long with a $\lambda/2$ frequency of 336 Hz. It can be viewed as consisting of 67, equally-spaced, hydrophone groups, with three missing groups spaced at quarter-length intervals along the array. A detailed description of the operating areas, the arrays, the on-line hardware and the recording system can be found in ref [1], along with the results of the on-line analysis.

(C) The results described in this report were obtained using a two-dimensional FFT beamformer which forms 64 beams and 154 frequency estimates at .2 Hz intervals in each 30 Hz band. Hanning shading was used in both the time and space domain. The 3 dB bandwidth at all frequencies is .29 Hz. Values of the 3 dB beamwidths for both array segments at different frequencies and azimuths are presented in Table A.1.....

MF Segment	0.°	30.°	60.°	70.°
30 Hz	5.2	6.0	10.5	16.5
60 Hz	2.6	3.0	5.2	7.7

HF Segment	0.°	30.°	60.°	70.°
275 Hz	3.0	3.5	6.0	9.0
305 Hz	2.7	3.1	5.4	8.0

Table A.1 (S). Beamwidths (3 dB) (U)

(U) The individual samples of the total beam power are formed by first averaging 21 consecutive beamformer outputs to yield a ten minute average. An interpolation procedure is then used to convert the beamformer variable to an azimuth variable after rotating in azimuth by the amount required to align the slightly different tow track headings to a common direction.

APPENDIX B

The Decomposition Algorithm (U)

(U) In this appendix we specify the algorithm used to decompose the total beam power, $B(\theta,f)$, into the sum of its spectral line component, $B_s(\theta,f)$, and its background component, $B_b(\theta,f)$. The algorithm, which is essentially the same as that used by Finny reference [3], has four key parameters. These parameters are identified and an analytical framework that can be used to evaluate their effect on the decomposition is developed.

(U) The decomposition algorithm is based on the principal that the spectral lines can be detected by comparing $B(\theta,f)$ against a threshold that is proportional to an estimate of the background power. This estimate, which is referred to here as the threshold power and is denoted by $B_T(\theta,f)$, is computed by averaging $B(\theta,f)$ over a deleted neighborhood of (θ,f), after first discarding the K_L largest and the K_S smallest values. The purpose of discarding these values is to reduce the bias in $B_T(\theta,f)$ due to the presence of spectral lines that occur in the neighborhood of (θ,f). If a line is detected at (θ,f), the spectral component is set equal to the difference between $B(\theta,f)$ and $B_T(\theta,f)$ and the background component is set equal to the threshold power. If no line is detected at (θ,f), the spectral line component equals zero and the background power equals the total power. In either case, the total power is the sum of the spectral component and the background component for all values of (θ,f).

(U) A precise specification is obtained as follows. Let B_i, B_{si} and B_{bi} be the total power, the spectral line power and the background power at the ith frequency-azimuth resolution cell (θ_i,f_i). For a fixed resolution cell, (θ_o,f_o), let $R_o = \{(\theta_i,f_i);\ i=1,\ldots,M\}$ denote a deleted neighborhood of (θ_o,f_o). Then the threshold power at (θ_o,f_o), B_{To}, is defined as

$$B_{To} = \left(\sum_{i=K_S+1}^{i=M-K_L} B_i' \right) / (M-(K_L+K_S)) \tag{B.1}$$

where the B_i' are the order statistics* of B_i, i=1,...,M. Finally,

*The B_i' are the reordering of B_i such that $B_1 \leq B_2 \leq \ldots \leq B_M$

(U) for a given threshold constant c, the spectral line component and background components at (θ_o, f_o) are defined by,

$$(B.2a) \quad B_{so} = \begin{cases} B_o - B_{To} & \text{if } B_o \geq c\, B_{To} \\ 0 & \text{otherwise} \end{cases}$$

and

$$(B.2b) \quad B_{bo} = \begin{cases} B_{To} & \text{if } B_o \geq c\, B_T \\ B_o & \text{otherwise} \end{cases}$$

(U) There are four basic parameters in the decomposition algorithm: the threshold constant (c), the shape of the region R_o, the number of points (M) in R_o and the numbers of large and small values that are discarded, (K_L) and (K_S). The spectral line and the background components described in Section 2 were obtained with c=1.8, $K_L = K_S = 1$, M=8 and

$$(B.3) \quad R_o = \{(\theta_o, f_i) \; ; \; i = \pm 1, \pm 3, \pm 5, \pm 7\}$$

Thus, the results in this report were obtained with B_{To} computed as an average of six values from a 2.93 Hz frequency band on each beam after first discarding the largest and the smallest values.

(U) In order to rigorously evaluate the effect of these parameters on the decomposition, it is necessary to specify the probability law on the total beam power at each frequency-azimuth resolution cell. It is then possible, at least in principal, to estimate the number of actual spectral lines present in $B(\theta, f)$ in terms of the number of spectral lines observed in $B_s(\theta, f)$. In particular, it can be shown that if $\hat{P}_s$ is the fraction of the (θ, f) plane occupied by actual spectral lines and P_s is the fraction of the (θ, f) plane for which $B_s(\theta, f)$ is non-zero, then

$$(B.4) \quad \hat{P}_s = (P_s/P_D)\,(1-P_F/P_s)/(1-P_F/P_D)$$

where P_D and P_F are the probabilities of detection and false alarm defined by,

$$(B.5a) \quad P_D = \text{Prob}\,[\, Z \geq c \mid \text{spectral line at } (\theta_o, f_o)]$$

$$(B.5b) \quad P_F = \text{Prob}\,[\, Z \geq c \mid \text{no spectral line at } (\theta_o, f_o)]$$

where $Z = B_o / B_{To}$

(U) Furthermore, the fraction of the non-zero portion of $B_s(\Theta, f)$ that corresponds to actual spectral lines and the fraction that results from the statistical variations in $B(\Theta, f)$ when no lines are present are equal to $P_D \hat{P}_s/P_s$ and $P_F (1-\hat{P}_s)/P_s$ respectively, where $\hat{P}_s$ is given by equation B.4.

(U) Ideally, the parameters of the decomposition algorithm should be chosen so that P_D is close to unity and P_F is very small. Then P_s will be approximately equal to $\hat{P}_s$ and $B_s(\Theta, f)$ will be an accurate representation of the spectral lines actually present in $B(\Theta, f)$. The effect of increasing the threshold constant is to reduce both P_D and P_F, and hence to reduce the number of lines observed in $B_s(\Theta, f)$. This effect has been observed in Figure 3.4. The computation required to rigorously evaluate this effect, as well as the effect of the remaining parameters, is beyond the scope of this report. Insead, we first derive bounds on the probabilities of detection and false alarm which can be used as the basis for further study. Secondly, a weak upper bound on the probability of false alarm is evaluated numerically by assuming that the beam power is distributed as a chi-squared random variable when no spectral lines are present. Finally, the effect of the shape of R_o is illustrated with several examples.

(U) The bounds on the probabilities of detection and false alarm are obtained as follows. Let p_n be the probability that exactly n resolution cells in R_o contain power from spectral lines and let $P_{D|n}$ and $P_{F|n}$ be the conditional probabilities of detection and false alarm defined by,

$$(B.6a) \quad P_{D|n} = \text{Prob}\left[Z \geq c \;\middle|\; \begin{array}{l}\text{spectral line at } (\Theta_o, f_o) \text{ and} \\ \text{spectral power at n cells in } R_o\end{array} \right]$$

$$(B.6b) \quad P_{F|n} = \text{Prob}\left[Z \geq c \;\middle|\; \begin{array}{l}\text{no spectral line at } (\Theta_o, f_o) \text{ and} \\ \text{spectral power at n cells in } R_o\end{array} \right]$$

Then P_D and P_F can be written as

$$(B.7a) \quad P_D = \sum_{n \geq 0} P_{D|n} \, P_n$$

$$(B.7b) \quad P_F = \sum_{n \geq 0} P_{F|n} \, P_n$$

Next, it is noted that both the condtional probabilities $P_{D|n}$ and $P_{F|n}$ are decreasing functions of n, since increasing the number of spectral lines in R_o can only increase B_{To}, and hence, must reduce the probability that B_o exceeds $c\, B_{To}$. It follows from

(U) this observation and equation (B-7b) that P_F satisfies,

$$P_{F|KL}\, P_{KL} \leq P_F \leq P_{F|o}\, P_{KL} + P_{F|KL+1}(1 - P_{KL}) \tag{B.7c}$$

where

$$P_{KL} = \sum_{n=o}^{K_L} P_n \tag{B.9}$$

with a similar ineqality for P_D.

(U) The bounds on P_F in the inequality (B.8) should be reasonably tight when K_L is large enough so that P_{KL} is close to unity. When this is the case, the second term on right-hand-side of (B.8) can be neglected. Furthermore, $P_{F|o}$ and $P_{F|KL}$ should be approximately equal, since the beam power in the resolution cells containing spectral lines should be discarded before computing the average. Thus, for large P_{KL}, $P_F \doteq P_{F|o}\, P_{KL}$ and a similar argument can be used to conclude that $P_D \doteq P_{D|o}\, P_{KL}$.

(U) To numerically evaluate the upper and lower bounds for P_D and P_F, it is necessary to specify p_n for n=o,..., K_L and to compute the conditional probabilities for n=o, K_L and K_L+1. These tasks require the specification of the probability law on the locations and the power in the spectral lines which is generally unknown apriori. Furthermore, when K_L and K_s are not zero, the computation of the conditional probabilities is complicated by the fact that the probability law on B_{To} is induced by the probability law on the order statistics of the B_i, as indicated in equation B.1. To alleviate these difficulties, we first note that since the conditional probabilities are decreasing function of n, the right-hand-side of B.7c is bounded above by $P_{F|o}$ and the left-hand-side is bounded below by $p_o\, P_{F|o}$. Thus, P_F also satisfies

$$p_o\, P_{F|o} \leq P_F \leq P_{F|o} \tag{B.10}$$

with a similar inequality for P_D. These bounds, although weaker than those in B.7c, require only the specification of p_o and the computation of the condtional probabilities given no spectral lines in R_o. Finally, it is noted that when K_L and K_s are approximately equal and no spectral lines occur in R_o, the probability law on M_{To} should be approximately the same as that

(U) induced directly by the probability law on the B_i. Thus, for K_L equals K_s, the conditional probabilities $P_{F|o}$ and $P_{D|o}$ can be approximated by viewing B_{To} as an average over $M-(K_L+K_S)$ points and otherwise neglecting the effect of discards.

(U) The upper bound on P_F is obtained by specifying the probability law on the total beam power given no spectral lines in R_o and computing $P_{F|o}$. For specific results we assume that the B_i are proportional to independent, identically distributed, chi-squared random variables with 2r degrees of freedom, where r is the number of samples in the time average used to obtain B_i. This assumption is consistent with a Gaussian noise field, independent time samples of beam power and points in R_o sufficiently separated so that the B_i are uncorrelated. It follows from this assumption that B_{To} is proportional to a chi-squared random variable on $2r(M-(K_L+K_S))$ degrees of freedom and that Z is F distributed with 2r and $2r(M-(K_L+K_S))$ degrees of freedom. Thus, $P_{F|o}$ can be evaluated for different threshold constants from tables of the F distribution. In particular, for 21 time samples and the parameters used in the decomposition algorithm P_F is bounded above by $P_{F|o} = .004$.

(U) We conclude this appendix with a discussion of the effect of the shape of R_o on the decomposition. This effect can be seen by viewing $B_T(\theta, f)$ as a smoothed version of $B(\theta, f)$. Then the spectral component is that part of $B(\theta, f)$ that exceeds $B_T(\theta, f)$ by the threshold constant and $B_b(\theta, f)$ is the difference between $B(\theta, f)$ and $B_s(\theta, f)$. In this context, the shape of R_o determines a two-dimensional filter on the (θ, f) plane* and its effect can be examined by considering the smoothing properties of this filter relative to the (θ, f) variations in $B(\theta, f)$.

(U) The plots of the total beam power in Section 2 suggest that the variations in $B(\theta, f)$ can be visualized in terms of three components: a component that is smooth in both θ and f, which represents the shipping noise that is not resolved**

* Strictly speaking the associated filter is data dependent due to the K_L+K_s discards.

**For a given noise field the relative contributions of the the three components depends on the array length and the analysis bandwidth.

(U) in θ and f; a component that is smooth in f but not in θ, which represents the frequency continuous portion of the spectra from noise sources that are resolved in θ ; and finally, a component that is smooth in neither θ or f, which represents the spectral lines from noise sources that are resolved in both θ and f.

(U) The shape of the region R_o used to obtain the results in the report, see equation B-3, represents one extreme, since this shape corresponds to a filter with frequency extent but no azimuth extent. The effect of this filter is to smooth the frequency variations in $B(\theta, f)$ while preserving the azimuthal variations. As a result, the decomposition algorithm tends to assign only the spectral lines to $B_s(\theta, f)$.

(U) At the other extreme, consider a region which has azimuthal extent but no frequency extent. Such a filter would smooth the azimuthal variations in $B(\theta, f)$ while preserving the frequency variations. With this filter, the decomposition algorithm tends to assign both the spectral lines and the frequency-continuous components to $B_s(\theta, f)$. This behavior is illustrated in Figures B-1 and B-2 which show $B_s(\theta, f)$ and $B_b(\theta, f)$ for sample one in the MF band with c=1.8, M=14, $K_L=K_S=2$ and

$$R_o = \{ (\theta_i, f_o) \ ; \ i = \pm 1, \ldots, \pm 7 \}$$

(U) The comparison of these plots with Figures 2.5 and 2.7 illustrates the difference in the results for the two extreme choices of the shape of R_o.

(U) As a final example, consider the region,

$$R_o = \{ (\theta_k, f_i) \ ; \ i = \pm 1, \pm 3, \pm 5, \pm 7 \ ; \ k = -1, 0, 1 \}$$

(U) This region has a small azimuth extent and the same frequency structure as the region of equation B.3. As a result, the corresponding filter smooths both the θ and f variations in $B(\theta, f)$. The spectral component for sample one in the MF band, obtained using this region with c=1.8, M=24 and $K_L=K_S=3$, is shown in Figure B.3. This plot is essentially the same as Figure 2.5, except that some of the spectral lines that are closely spaced in azimuth and are not totally separated in Figure 2.5, are totally separated in Figure B.3. This example suggests that some azimuthal extent in R_o can improve the resolution of the spectral lines while keeping the frequency-continuous portion of the spectra in $B_b(\theta, f)$

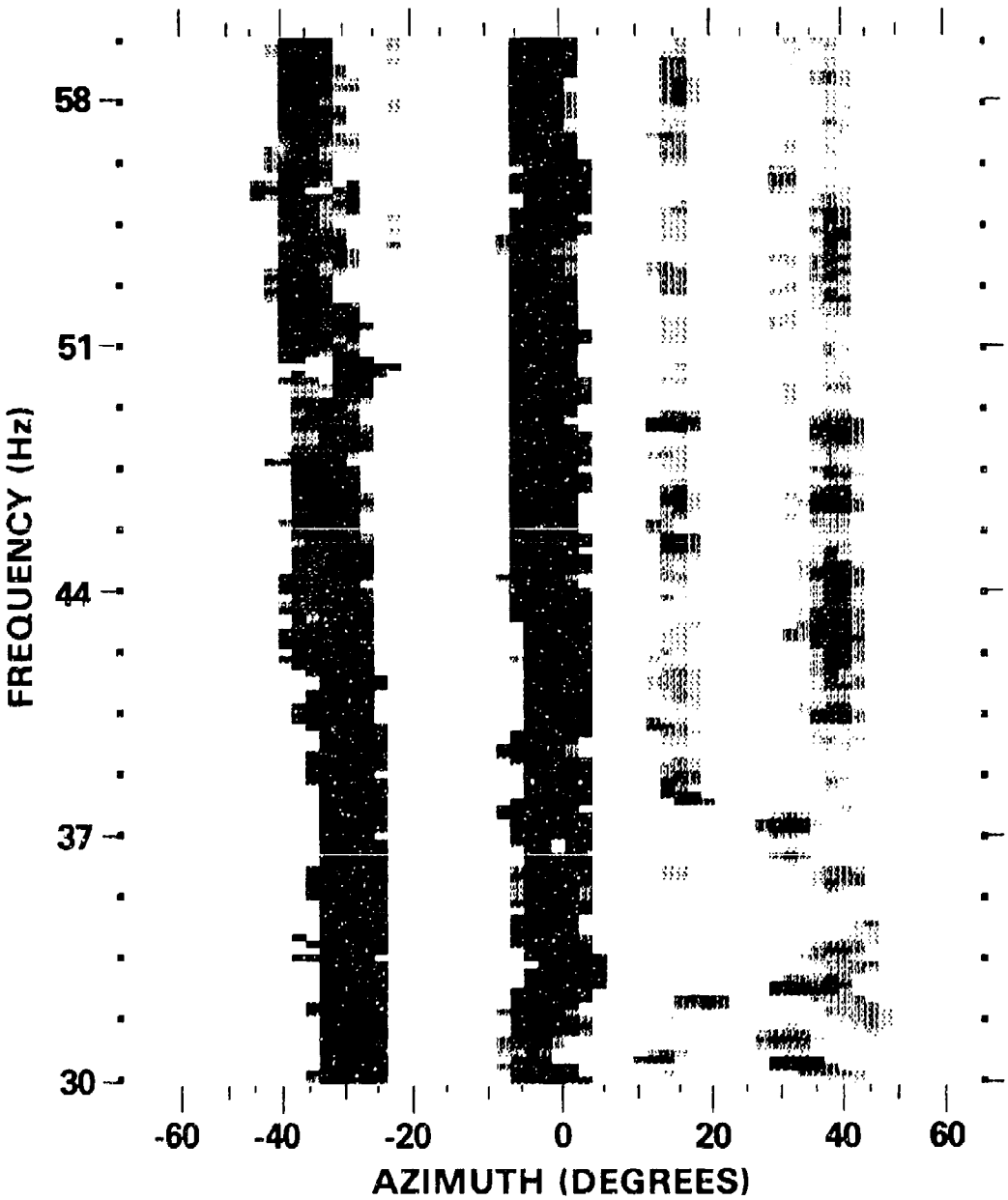

Fig. B.1 (C) — Spectral line component; azimuth smoothing only, 56-74 dB//uPa; MF band, sample one (U)

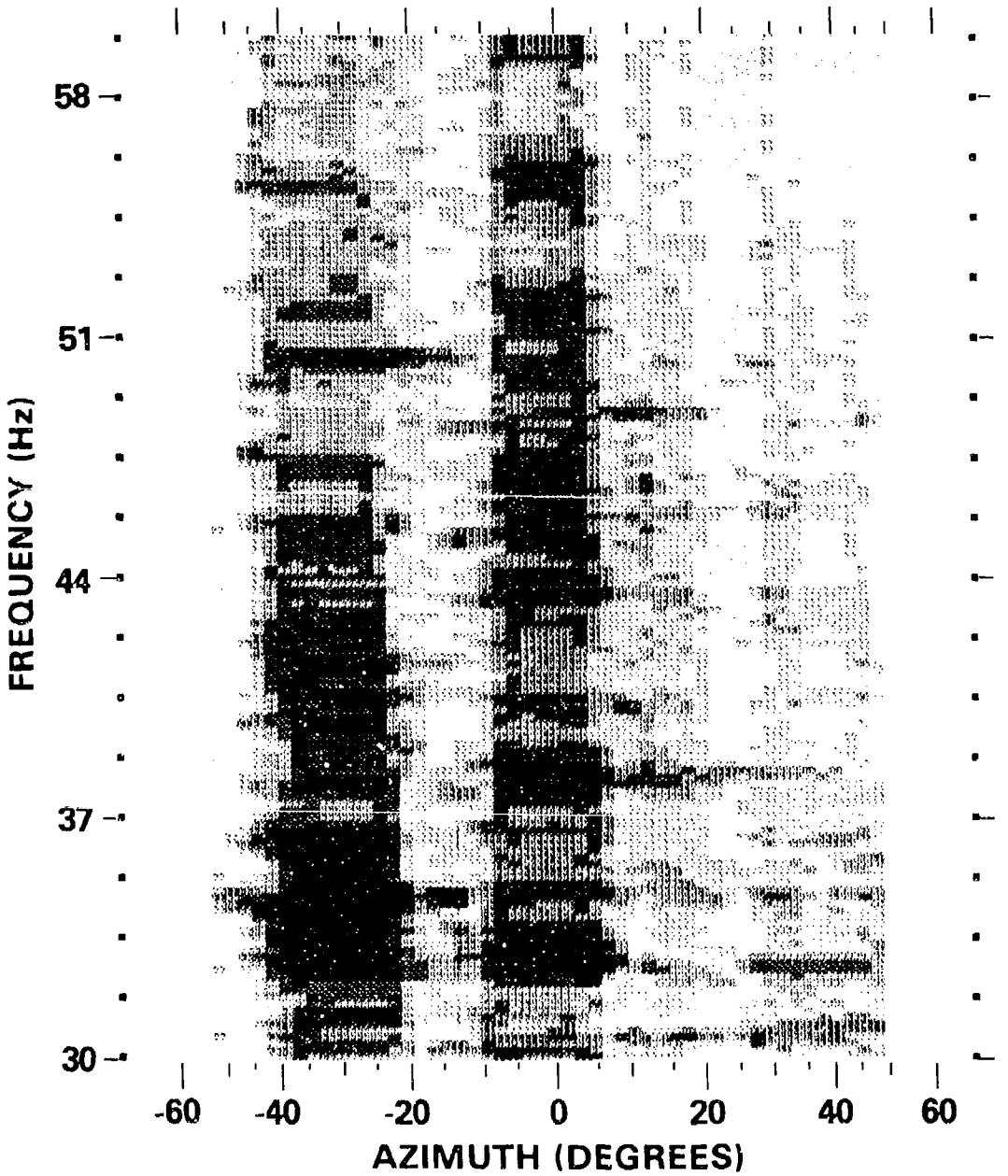

Fig. B.2 (C) — Background component; azimuth smoothing only, 56-57 dB//uPa; MF band, sample one (U)

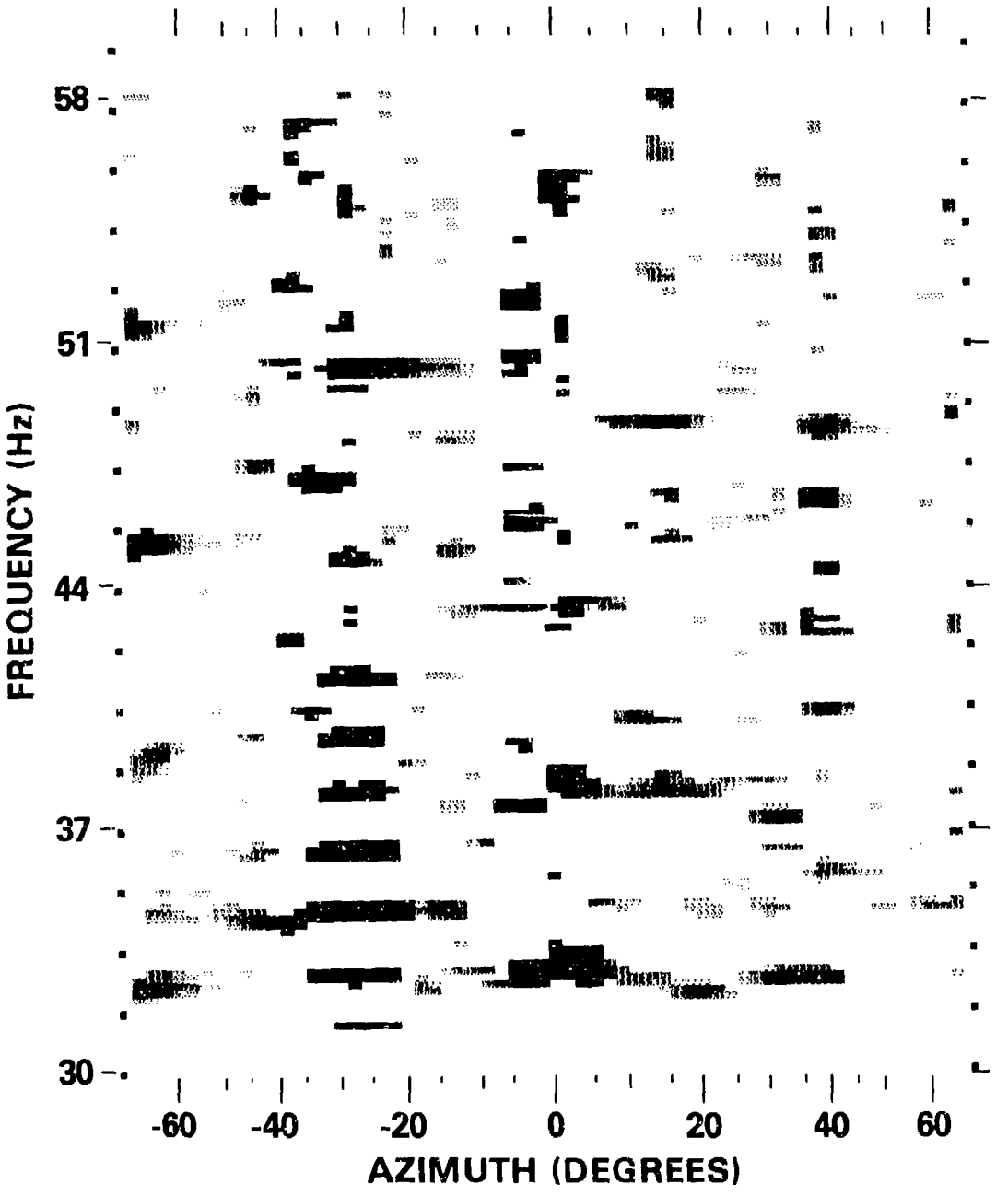

Fig. B.3 (C) — Spectral line component; both azimuth and frequency smoothing, 56-74 dB//uPa; MF band sample one (U)

APPENDIX C

An Algorithm for Reducing the Effect of Missing Hydrophones (U)

(U) The HF array segment can be viewed as an array of 67, equally-spaced, hydrophones* with three missing hydrophones located at approximately quarterlength intervals along the array. The effect of these missing hydrophones is to increase the peak sidelobe levels of the beam response to a spatially coherent signal to within 24 dB of the maximum beam value. This does not significantly alter the azimuthal distribution of the beam power at frequencies where no strong coherent signals are present. However, at those frequencies with coherent signals that yield beam signal-to-noise ratios in excess of 24 dB, the azimuthal distribution of the beam power will be dominated by the sidelobe levels over the full 180 degree azimuthal sector. In this Appendix, we specify the algorithm that was used to reduce the sidelobe levels due to the missing hydrophones and show an example illustrating the difference in the beam response obtained using the algorithm and that obtained by beamforming using only the hydrophones that are actually present.

(U) The algorithm computes an estimate of the complex amplitude for each missing hydrophone using the complex amplitudes from the four neighboring hydrophones. The amplitude estimate is computed as an average of the amplitudes of the four neighboring hydrophones. The estimate of the phase factor is computed by first forming two estimates, each involving three of the four neighboring hydrophones, and then combining these estimates to obtain the average phase factor. Finally, conventional frequency-domain beamforming is applied to the augmented set of complex amplitudes.

(U) A detailed specification of the estimation procedure is as follows. Let Z_i be the complex amplitude of the i^{th} hydrophone and let $\hat{Z}_{io}$ be the estimate of the complex amplitude of the missing hydrophone i_o. Then the amplitude $|\hat{Z}_{io}|$ is computed as,

$$(C\text{-}1) \qquad |\hat{Z}_{io}| = (|Z_{io-2}| + |Z_{io-1}| + |Z_{io+1}| + |Z_{io+2}|)/4$$

and the phase factor, $\exp\{j\theta_{io}\}$ is computed as,

$$(C\text{-}2a) \qquad \exp\{j\theta_{io}\} = (W_m+W_p)/(|W_m + W_p|)$$

*The "hydrophones" referred to in this appendix are actually groups of individual hydrophone elements.

(U) where

$$(C\text{-}2b) \quad W_m = (Z_{io-2} \quad Z_{io+1} \quad Z^{*}_{io-1}) / |Z_{io-2} \quad Z_{io+1} \quad Z_{io-1}|$$

$$(C\text{-}2c) \quad W_p = (Z_{io+2} \quad Z^{*}_{io+1} \quad Z_{io-1}) / |Z_{io+2} \quad Z_{io+1} \quad Z_{io-1}|$$

(U) It is noted that the computations involve only the complex amplitudes and their magnitudes. This is done to avoid the 2π ambiguity that arises in computations on the phases associated with the complex amplitudes.

(U) The algorithm can be explained in hueristic terms as follows. Consider first, those frequencies where a strong spatially ccherent signal is present. At these frequencies, the amplitude distribution in the vicinity of the missing hydrophone will be approximately constant and the phase distribution will be nearly linear. When this is the case, the estimate will approximate the true complex amplitude at the missing hydrophone and the sidelobe levels due to the strong coherent signal will be significantly reduced. To see this, assume that Z_i can be represented as

$$(C\text{-}4) \quad Z_i = |Z_i| \exp\{j(Ki + \varphi_i)\}$$

where Ki is the phase due to the coherent signal, with K depending on both the frequency and the incident angle, and φ_i is the contribution due to noise. Substitution of (C-4) into (C-2), and some algebraic manipulation, yields,

$$(C\text{-}5a) \quad \exp\{j\theta_{io}\} = \exp\{j(Ki_o + \varphi_e)\}$$

where

$$(C\text{-}5b) \quad \varphi_e = (\varphi_{i-2} + \varphi_{i+2})/2 + \alpha$$

$$(C\text{-}5c) \quad \alpha = \begin{cases} 0 & \text{if } \cos[(\varphi_{i-2} - \varphi_{i+2})/2 + (\varphi_{i+1} - \varphi_{i-1})] \geq 0 \\ \pi & \text{otherwise} \end{cases}$$

For large signal-to-noise ratios, α will almost always be zero, φ_e will generally be small, and hence, $\exp\{j\theta_{io}\}$ will approximate the true phase factor. Furthermore, the amplitude

(U) of the estimate, which is computed according to equation (C-1), will also approximate the true amplitude. Thus, the beam response obtained by beamforming on the augmented set of complex amplitudes will have sidelobe levels that approximate those that would result if the missing hydrophones were present.

(U) Next consider those frequencies where no strong spatially coherent signal is present. At these frequencies, both the amplitude and the phase factor of the estimate may differ signifcantly from the true values at any given time. The amplitude of the estimate will be roughly equal to the mean amplitude due to the noise alone and the phase of the estimate, relative to the true value, will be approximately distributed as a uniform random variable. However, the correlation between the phase factor of the estimate and those corresponding to the neighboring hydrophones will be small. Thus, the beam response obtained using the augmented set of compelx amplitudes will again be approximately the same, in the average, as is if the missing hydrophones were present.

(U) A rigorous performance evaluation of the algorithm requires the specification of the probability laws on both the signal and the noise fields and the computation of the mean sidelobe level obtained using the estimation procedure. This computation, which is complicated by the fact that the estimation procedure is nonlinear, is beyond the scope of this appendix. In lieu of this evaluation, we illustrate both the need for and the effect of the algorithm, by comparing the beam power from sample one on the HF array segment obtained using the algorithm, against that obtained by beamforming using only the hydrophones that are actually present. The plots of the total beam power for both cases are illustrated in Figures C-1 and C-2, where the scale on beam power in each plot ranges from 38 dB down from the peak value of the 280 Hz signal line to 20 dB down from the peak, in 3 dB steps per shade.

(U) The plot of the total beam power obtained without using the algorithm, Figure C-1, illustrates the effect of the missing hydrophones on the total beam power.* At several frequencies, the sidelobe levels associated with strong coherent signals completely dominate the beam power over the full 180 degrees. This is most evident at the 280 Hz signal frequency, although there are other frequencies where the array tow ship noise is sufficiently large to mask the azimuthal distribution of the beam power due to noise sources other than the array tow ship.

*The beam power in Figure C.1, is obtained using Hanning shading on 64 hydrophones with zero coefficients at the positions of the missing hydrophones.

(U) Figure (C-2) illustrates the beam power obtained by including the estimates of the complex amplitudes in the input to the beamformer.* A comparison of Figures (C-2) and (C-1), shows that the sidelobe levels associated with the strong coherent signals have been reduced significantly. This is particularly evident in the low noise directions (in the vicinity of ± 50 degrees), where the beam noise is essentially uncontaminated by the sidelobes from the 280 Hz signal and the array tow ship noise.

(U) A more detailed comparison of the effect of the algorithm can be seen in Figures (C-3) and (C-4) where we have plotted the azimuthal distribution of the beam power at 280 Hz and at 276.6 Hz. The continuous line curve in each plot represents the beam power obtained by neglecting the missing hydrophones and the dotted curve represents the beam power obtained using the algorithm. The beam power in both plots is normalized to the maximum beam power at the 280 Hz signal line.

(U) The azimuthal power distributions at 280 Hz, illustrated in Figure C-3, shows that the effect of the algorithm is to significantly reduce the beam power at all azimuths except those where spatially coherent signals are actually present.** This reduction is most dramatic in the low noise directions where the two curves differ by as much as 9dB.

(U) The azimuthal power distributions at 276.6 Hz, Figure C-4, shows that even without the 280 Hz signal line, the reduction in the beam noise at azimuths where no dominant coherent source is present can be significant. The difference between the two curves is somewhat less than that in Figure C-3, except near -50 degrees where the two differences are comparable.

---

* Three hydrophones were dropped from the ends of the augmented set so that an FFT algorithm on 64 points could be used for beamforming.

**Less than .6 dB of the difference between the two curves can be attributed to the fact that the scale for each curve is relative to the peak of the 280 Hz signal line.

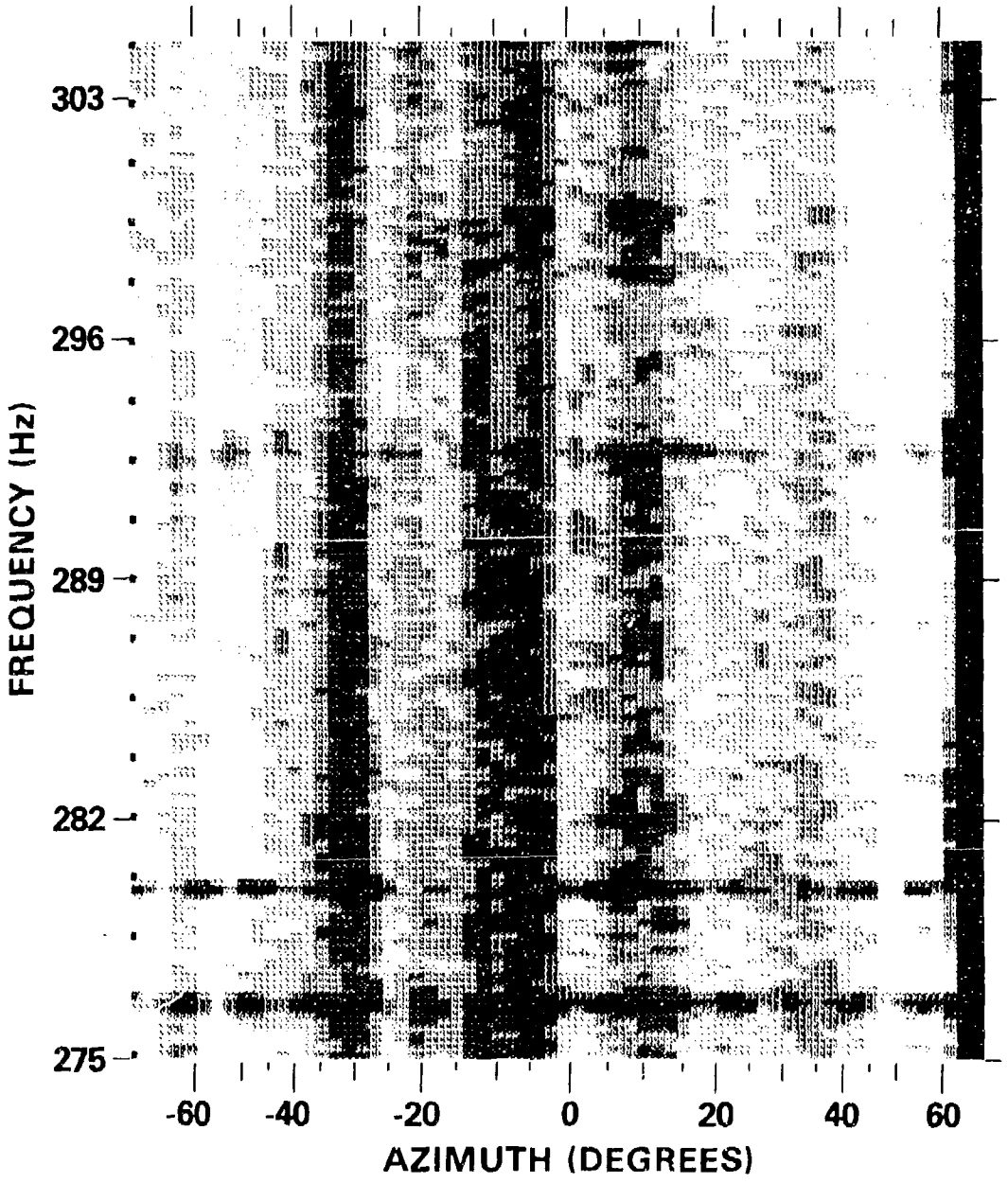

Fig. C.1 (C) — Beam power obtained using only hydrophone present, 40.5-58.5 dB//uPa; HF band, sample one (U)

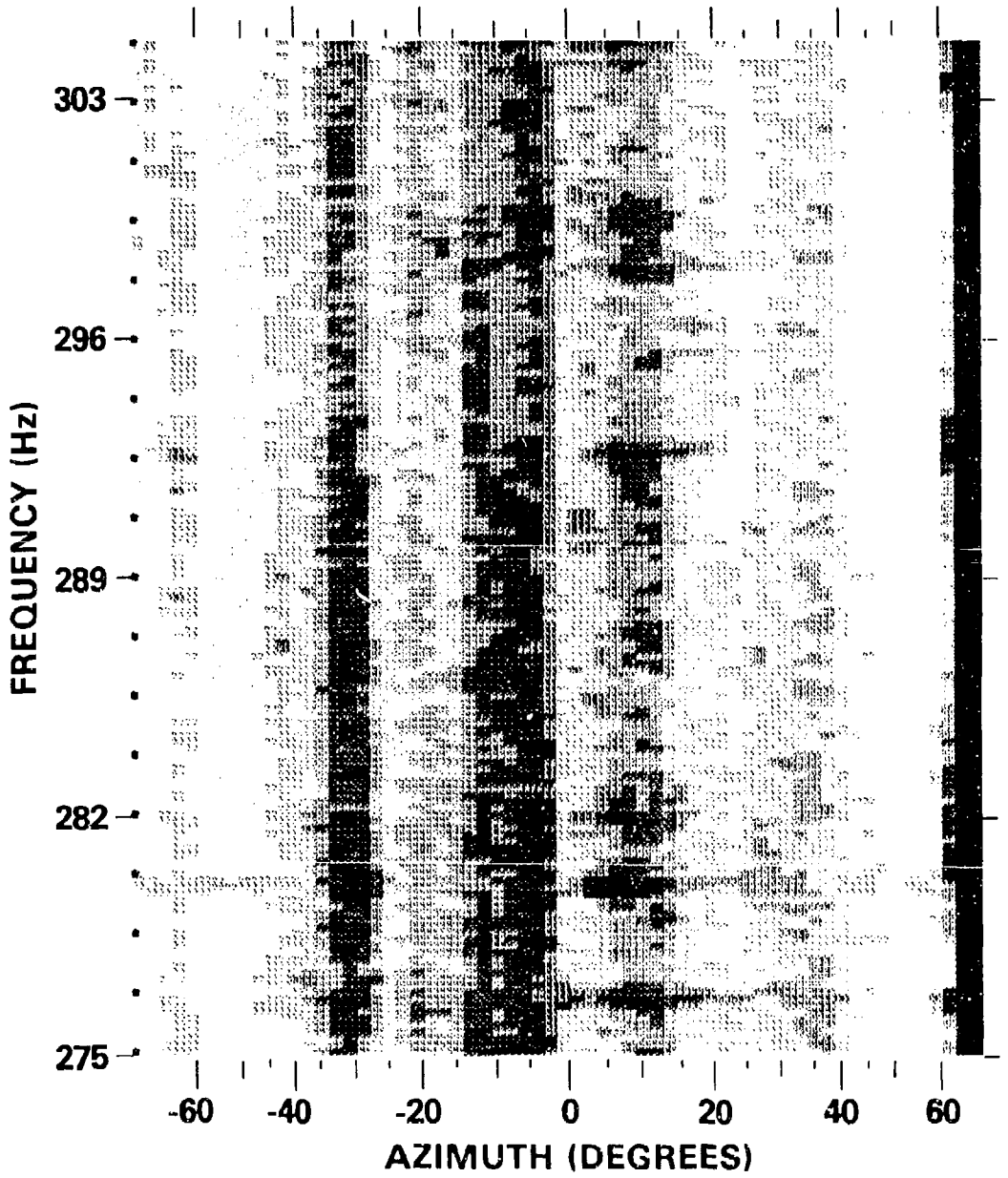

Fig. C.2 (C) — Beam power obtained using estimates for missing hydrophones, 41-59 dB//uPa HF band, sample one (U)

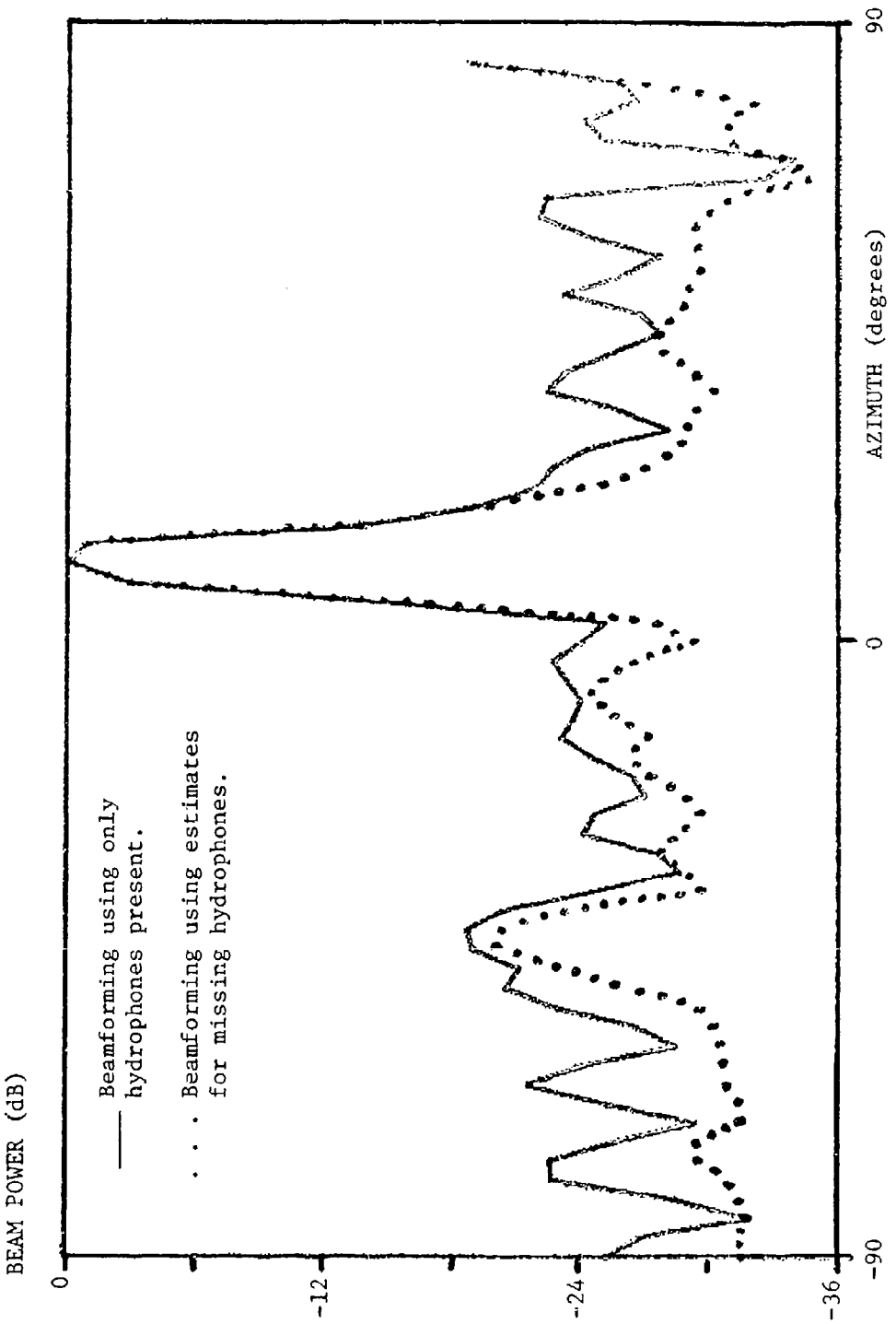

Fig. C.3 (C) — Azimuthal power distribution at 275 Hz (U)

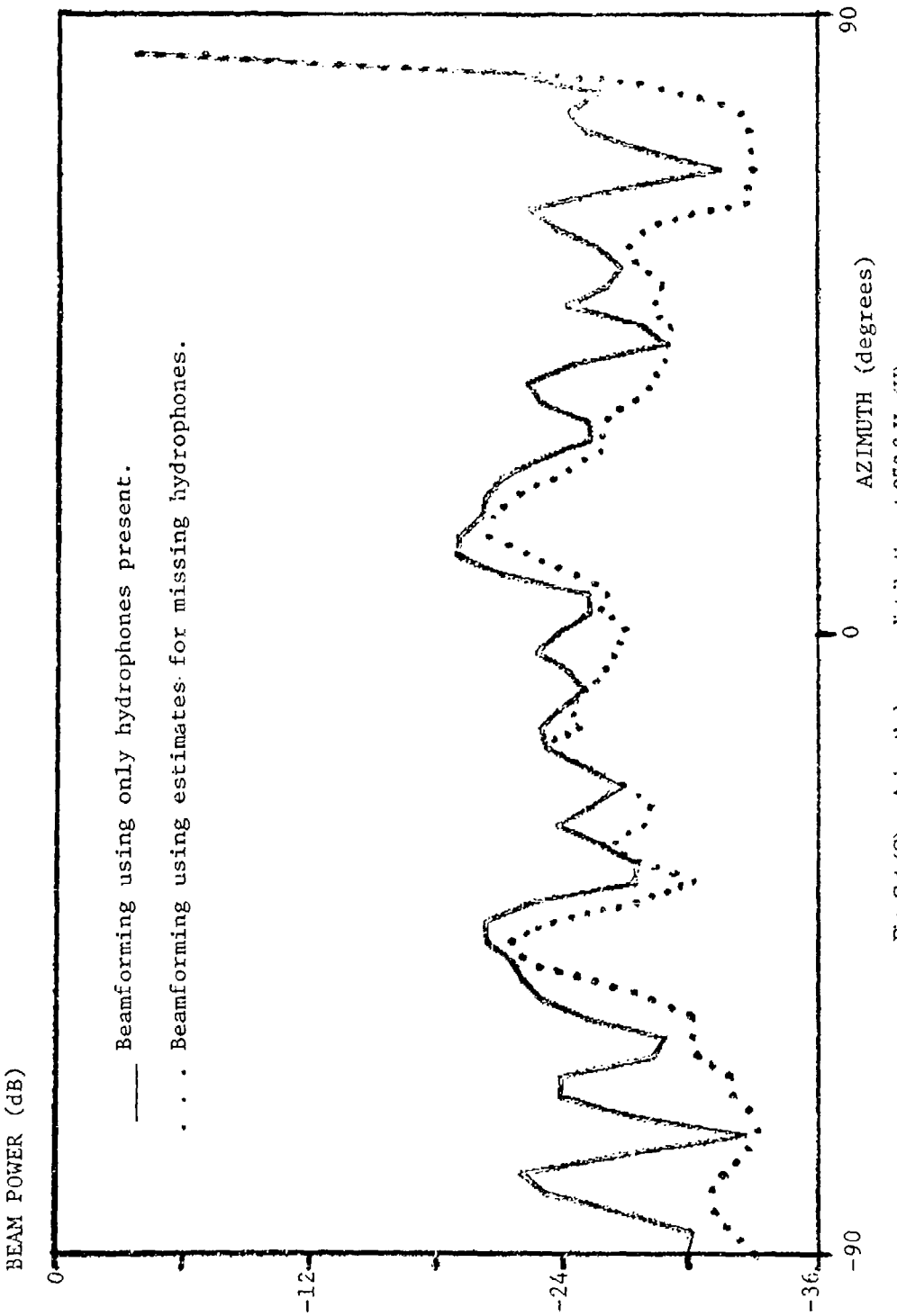

Fig. C.4 (C) – Azimuthal power distribution at 276.6 Hz (U)

This Page Intentionally Blank

DISTRIBUTION LIST

Assistant Secretary of the Navy (RE&S) Washington, D.C. 20301	
Attn: G.A. Cann	1
Chief of Naval Operations Department of the Navy Washington, D.C. 20350	
Attn: OP-095	1
OP-951	1
OP-955	1
Chief of Naval Development Headquarters, Naval Material Command Washington, D. C. 20360 Attn: MAT-035	1
Commander David M. Taylor Naval Ship Research and Development Center Bethesda, Md. 20034	1
Commander Naval Air Development Center Warminster, Pa. 18974	2
Commander in Chief U. S. Atlantic Fleet Norfolk, Va. 23511	1
Commander Oceanographic Systems, Atlantic Box 100 Norfolk, Va. 23511	2
Chief of Naval Research Department of the Navy Arlington, Va. 22217 Attn: Dr. J . B. Hersey	1

Oceanographer of the Navy
Hoffman Building II
200 Stovall Street
Alexandria, Va. 22332
Attn: CDR E. T. Young 1

Commander
Naval Air Systems Command
Department of the Navy
Washington, D. C. 20360
Attn: Code PMA-264 1

Commander
Naval Electronic Systems
Command
Department of the Navy
Washington, D. C. 20360
Attn: PME-124 - 40 - 60 3
ELEX-320 1
ELEX-035 1

Commander
Naval Sea Systems Command
Department of the Navy
Washington, D. C. 20362
Attn: SEA-06H1 1

Strategic Systems Project
Office
Department of the Navy
Washington, D. C. 20360 1

Anti Submarine Warfare
Systems Project Office
Department of the Navy
Washington, D. C. 20360 2

Commanding Officer and Director
Defense Documentation Center
Defense Services Administration
Cameron Station, Bldg. 5
5010 Duke Street
Alexandria, Va. 22314 1

Commander 1
Naval Ocean Systems Center
San Diego, CA 92132
Attn: M. R. Akers 2
Dr. E. B. Tunstall 1
R. R. Gardner 1

Commander Naval Underwater Systems Center New London Laboratory New London, CT 06320 Attn: R. L. Martin	4
Commander Naval Oceanographic Office Department of the Navy Washington, D. C. 20373 Attn: J. L. Kerling	1
Director for Naval Matters Center for Naval Analysis Arlington, Va 22209 Attn: C. E. Woods	1 1
Commanding Officer Naval Ocean Research and Development Activity NSTL Station, MS 39529	1
Attn: Code 110	1
Code 200	1
Code 300	1
Code 320	1
Code 340	1
Code 400	1
Code 500	1
Code 600	3
NORDA Liaison Office Office of Naval Research Arlington, VA 22217 Attn: K. W. Lackie	2
Defense Advanced Research Projects Agency 1400 Wilson Boulevard Arlington, VA. 22209	1
ARPA Research Center Unit 1, Bldg. 301A NAS Moffett Field, CA 94035 Attn: E. L. Smith	1
Analysis & Technology, Inc. Rt 2 North Stonington, CT 06359 Attn: S. Elam	1

Applied Physics Laboratory
Johns Hopkins University
Johns Hopkins Road
Laurel, Md. 20810
Att: Dr. G. L. Smith 1

Applied Research Laboratories
University of Texas
P. O. Box 8029
Austin, Texas 78712
Attn: G. E. Ellis 1
Dr. L. D. Hampton 1

Arthur D. Little, Inc.
15 Acord Park
Cambridge, MA. 02140
Attn: W. G. Sykes 1

Bolt, Beranek, and Newman
1701 N. Fort Myer Drive
Suite 1001
Arlington, VA 22209 1

Bell Telephone Laboratories 1
1 Whippany Road
Whippany, N. J. 07981

Daniel H. Wagner Associates 1
Station Square One
Paoli, PA 19301

Daubin Systems Corporation 1
104 Crandon Blvd.
Suite 315
Key Biscayne, Fl 33149

University of California, San Diego
Marine Physical Laboratory of the
Scripps Inst. of Oceanography
San Diego, CA 92132
Attn: V. C. Anderson 1

Operations Research, Inc.
1400 Spring Street
Silver Spring, MD 20910
Attn: Dr. J. K. Bowen 1

Planning Systems, Inc.
7900 Westpark Drive
McLean, VA 22101
Attn: Dr. L. P. Solomon 1

UNCLASSIFIED

Raytheon Company
Submarine Signal Division
P. O. Box 360
Portsmouth, RI 02871
Attn: Dr. B. A. Becken 1

Science Applications, Inc.
4422/8400 Westpark Drive
McLean, VA 22101
Attn: Dr. J. S. Hanna 1

Sutron Corporation
1921 N. Lynn Street
Suite 700
Alexandria, VA 22209
Attn: C. H. Dabney 1

Tetra Tech, Inc.
1911 Fort Meyer Drive
Arlington, VA 22209
Attn: W. E. Sims 1

Texas Instruments, Inc.
P. O. Box 6015
Dallas, Texas 75222
Attn: A. Kirst, Jr. 1

Tracor, Inc.
1601 Research Blvd.
Rockville, MD 20850
Attn: J. T. Gottwald 1

TRW Systems Group
7600 Colshire Drive
McLean, VA. 22101
Attn: R. T. Brown 1
I. B. Gereben 1

Undersea Research Corporation
7777 Leesburg Pike, Suite 305
Falls Church, VA 22043
Attn: V. F. Anderson 1

Underwater Systems, Inc.
World Building
8121 Georgia Avenue
Silver Spring, Md. 20910
Attn: Dr. M. S. Weinstein 1

Western Electric Company 2400 Reynilds Road Winston-Salem, N.C. 27106	1
Woods Hole Oceanographic Institution Woods Hole, Mass. 02543 Attn: E.E. Hays	1
Xonics, Inc. 6837 Hayvenhurst Avenue Van Nuys, Calif. 91406 Attn: S. Kulek	1
Naval Research Laboratory Code 8160 Washington, D. C. 20375	1

UNITED STATES GOVERNMENT

Memorandum

7100-034

DATE: 26 February 2004

REPLY TO ATTN OF: Burton G. Hurdle (Code 7103)

SUBJECT: REVIEW OF REF (A) FOR DECLASSIFICATION

TO: Code 1221.1

REF: (a) "Preliminary Results of an Analysis of Beam Noise in the Mediterranean" (U), R. Heitmeyer and G. Long, Acoustics Division, NRL Memo Report 3832, September 1978 (S)

1. Reference (a) is a report of the preliminary results of an experiment to measure beam noise in two frequency bands (30-60 and 275-305). The results indicate that the noise is primarily due to shipping

2. The technology and equipment of reference (a) have long been superseded. The current value of these papers is historical

3. Based on the above, it is recommended that reference (a) be declassified and released with no restrictions

Burton G. Hurdle

BURTON G. HURDLE
NRL Code 7103

CONCUR:

Edward R. Franchi 3/1/2004

E.R. Franchi Date
Superintendent, Acoustics Division

CONCUR:

Tina Smallwood 3/3/04

Tina Smallwood Date
NRL Code 1221.1

DEPARTMENT OF THE NAVY
OFFICE OF NAVAL RESEARCH
875 NORTH RANDOLPH STREET
SUITE 1425
ARLINGTON VA 22203-1995

IN REPLY REFER TO:

5510/1
Ser 321OA/011/06
31 Jan 06

MEMORANDUM FOR DISTRIBUTION LIST

Subj: DECLASSIFICATION OF LONG RANGE ACOUSTIC PROPAGATION PROJECT (LRAPP) DOCUMENTS

Ref: (a) SECNAVINST 5510.36

Encl: (1) List of DECLASSIFIED LRAPP Documents

1. In accordance with reference (a), a declassification review has been conducted on a number of classified LRAPP documents.

2. The LRAPP documents listed in enclosure (1) have been downgraded to UNCLASSIFIED and have been approved for public release. These documents should be remarked as follows:

   Classification changed to UNCLASSIFIED by authority of the Chief of Naval Operations (N772) letter N772A/6U875630, 20 January 2006.

   DISTRIBUTION STATEMENT A: Approved for Public Release; Distribution is unlimited.

3. Questions may be directed to the undersigned on (703) 696-4619, DSN 426-4619.

BRIAN LINK
By direction

Subj: DECLASSIFICATION OF LONG RANGE ACOUSTIC PROPAGATION PROJECT (LRAPP) DOCUMENTS

DISTRIBUTION LIST:

NAVOCEANO (Code N121LC – Jaime Ratliff)
NRL Washington (Code 5596.3 – Mary Templeman)
PEO LMW Det San Diego (PMS 181)
DTIC-OCQ (Larry Downing)
ARL, U of Texas
Blue Sea Corporation (Dr.Roy Gaul)
ONR 32B (CAPT Paul Stewart)
ONR 321OA (Dr. Ellen Livingston)
APL, U of Washington
APL, Johns Hopkins University
ARL, Penn State University
MPL of Scripps Institution of Oceanography
WHOI
NAVSEA
NAVAIR
NUWC
SAIC

Declassified LRAPP Documents

Report Number	Personal Author	Title	Publication Source (Originator)	Pub. Date	Current Availability	Class.
Unavailable	Bossard, David C.	ACOUSTIC ANALYSIS/ASEPS	Wagner Associates	780726	ADA076268	U
NRLMR3832	Heitmeyer, R., et al.	PRELIMINARY RESULTS OF AN ANALYSIS OF BEAM NOISE IN THE MEDITERRANEAN (U)	Naval Research Laboratory	780901	ADC016220 ND	U
Unavailable	Watrous, B. A.	PARKA 1 OCEANOGRAPHIC DATA COMPENDIUM	Naval Ocean R&D Activity	781101	ADB115967	U
Unavailable	Dunbar, B., et al.	LAMBDA PROCESSING LABORATORY AND ENGINEERING SUPPORT, FINAL REPORT 1 JANUARY 1977 - 31 OCTOBER 1978	Texas Instruments, Inc.	781129	ND	U
Unavailable	Blumen, L. S., et al.	ASTRAL MODEL. VOLUME 2: SOFTWARE IMPLEMENTATION	Science Applications, Inc.	790101	ADA956122	U
Unavailable	Spofford, C. W.	ASTRAL MODEL. VOLUME 1: TECHNICAL DESCRIPTION	Science Applications, Inc.	790101	ADA956124	U
Unavailable	Townsend, R., et al.	SELF-TENSIONING ACOUSTICAL HORIZONTAL LINE ARRAY (SPRAY) DATA ANALYSIS. FINAL REPORT OF BEARING STAKE TESTS JANUARY THRU MARCH 1977. VOLUME IA. OVERALL PROGRAM PERFORMANCE RESULTS WITH TEST RESULTS SUMMARY	Sanders Associates, Inc.	790101	ADC017573	U
Unavailable	Unavailable	SELF-TENSIONING ACOUSTICAL HORIZONTAL LINE ARRAY (SPRAY) DATA ANALYSIS. FINAL REPORT OF BEARING STAKE TESTS JANUARY THRU MARCH 1977. VOLUME IB. DETAILED DESCRIPTION, TEST RESULTS	Sanders Associates, Inc.	790101	ADC017574	U
Unavailable	Unavailable	SELF-TENSIONING ACOUSTICAL HORIZONTAL LINE ARRAY (SPRAY) DATA ANALYSIS. FINAL REPORT OF BEARING STAKE TESTS JANUARY THRU MARCH 1977. VOLUME II. DATA ANALYSIS FACILITY AND DATA REDUCTION METHODOLOGY	Sanders Associates, Inc.	790109	ADC017575	U
Unavailable	Unavailable	SELF-TENSIONING ACOUSTICAL HORIZONTAL LINE ARRAY (SPRAY) DATA ANALYSIS. FINAL REPORT OF BEARING STAKE TESTS JANUARY THRU MARCH 1977. VOLUME IIIA. DATA POINTS 1, 2 AND 3 RAW DATA	Sanders Associates, Inc.	790109	ADC017576	U
Unavailable	Unavailable	SELF-TENSIONING ACOUSTICAL HORIZONTAL LINE ARRAY (SPRAY) DATA ANALYSIS. FINAL REPORT OF BEARING STAKE TESTS JANUARY THRU MARCH 1977. VOLUME IIIB. DATA POINTS 4, 5 AND 6 RAW DATA	Sanders Associates, Inc.	790109	ADC017577	U
Unavailable	Unavailable	SELF-TENSIONING ACOUSTICAL HORIZONTAL LINE ARRAY (SPRAY) DATA ANALYSIS. FINAL REPORT OF BEARING STAKE TESTS JANUARY THRU MARCH 1977. VOLUME IVA. DATA POINTS 7, 8 AND 9 RAW DATA	Sanders Associates, Inc.	790109	ADC017578	U